formerly Typeset

Open access • Posted Content • DOI:10.1101/694869

STARRPeaker: Uniform processing and accurate identification of STARR-seq active regions — Source link

Dong-Hoon Lee, Manman Shi, Jennifer R. Moran, Martha Wall ...+7 more authors

Institutions: Yale University, University of Chicago, Westlake University

Published on: 20 Jul 2019 - bioRxiv (Cold Spring Harbor Laboratory)

Topics: STARR-seq and Enhancer

Related papers:

- STARRPeaker: Uniform processing and accurate identification of whole human STARR-seq active regions
- Variant analysis pipeline for accurate detection of genomic variants from transcriptome sequencing data.
- Variant Analysis Pipeline for Accurate Detection of Genomic Variants from Transcriptome Sequencing Data: SNP Calling from RNA-seq Data in Non-Human Models
- Correcting nucleotide-specific biases in high-throughput sequencing data
- Elimination of PCR duplicates in RNA-seq and small RNA-seq using unique molecular identifiers

Share this paper:

View more about this paper here: https://typeset.io/papers/starrpeaker-uniform-processing-and-accurate-identification-3fcv3vkktq

bioRxiv preprint doi: https://doi.org/10.1101/694869; this version posted May 5, 2020. The copyright holder for this preprint (which was not certified by peer review) is the author/funder, who has granted bioRxiv a license to display the preprint in perpetuity. It is made available under aCC-BY-NC-ND 4.0 International license.

1 # STARRPeaker: Uniform processing and accurate identification of
2 # STARR-seq active regions

3

4 Donghoon Lee[1,2], Manman Shi[3], Jennifer Moran[3], Martha Wall[3], Jing Zhang[1,2], Jason
5 Liu[2], Dominic Fitzgerald[3], Yasuhiro Kyono[3], Lijia Ma[3,4], Kevin P White[3,5]*, Mark
6 Gerstein[1,2,6,7]*

7

8 [1] Program in Computational Biology and Bioinformatics, Yale University, New Haven,
9 CT 06520, USA
10 [2] Department of Molecular Biophysics and Biochemistry, Yale University, New Haven,
11 CT 06520, USA
12 [3] Institute for Genomics and System Biology, University of Chicago, Chicago, IL 60637,
13 USA
14 [4] School of Life Sciences, Westlake University, Hangzhou, Zhejiang 310024, China
15 [5] Tempus Labs, Inc., Chicago, IL 60654, USA
16 [6] Department of Computer Science, Yale University, New Haven, CT 06520, USA
17 [7] Department of Statistics and Data Science, Yale University, New Haven, CT 06520,
18 USA
19 * Corresponding authors

20

21 E-mail: pi@gersteinlab.org

22

23 ## Abstract

bioRxiv preprint doi: https://doi.org/10.1101/694869; this version posted May 5, 2020. The copyright holder for this preprint (which was not certified by peer review) is the author/funder, who has granted bioRxiv a license to display the preprint in perpetuity. It is made available under aCC-BY-NC-ND 4.0 International license.

24 **Background**: High-throughput reporter assays, such as self-transcribing active
25 regulatory region sequencing (STARR-seq), allow for unbiased and quantitative
26 assessment of enhancers at a genome-wide scale. Recent advances in STARR-seq
27 technology have employed progressively more complex genomic libraries and
28 increased sequencing depths, to assay larger sized regions, up to the entire human
29 genome. These advances necessitate a reliable processing pipeline and peak-calling
30 algorithm.

31 **Results**: Most STARR-seq studies have relied on chromatin immunoprecipitation
32 sequencing (ChIP-seq) processing pipelines. However, there are key differences in
33 STARR-seq versus ChIP-seq. First, STARR-seq uses transcribed RNA to measure the
34 activity of an enhancer, making an accurate determination of the basal transcription rate
35 important. Second, STARR-seq coverage is highly non-uniform, overdispersed, and
36 often confounded by sequencing biases, such as GC content and mappability. Lastly,
37 here, we observed a clear correlation between RNA thermodynamic stability and
38 STARR-seq readout, suggesting that STARR-seq may be sensitive to RNA secondary
39 structure and stability. Considering these findings, we developed a negative-binomial
40 regression framework for uniformly processing STARR-seq data, called STARRPeaker.
41 In support of this, we generated whole-genome STARR-seq data from the HepG2 and
42 K562 human cell lines and applied STARRPeaker to call enhancers.

43 **Conclusions**: We show STARRPeaker can unbiasedly detect active enhancers from
44 both captured and whole-genome STARR-seq data. Specifically, we report ~33,000 and
45 ~20,000 candidate enhancers from HepG2 and K562, respectively. Moreover, we show
46 that STARRPeaker outperforms other peak callers in terms of identifying known

bioRxiv preprint doi: https://doi.org/10.1101/694869; this version posted May 5, 2020. The copyright holder for this preprint (which was not certified by peer review) is the author/funder, who has granted bioRxiv a license to display the preprint in perpetuity. It is made available under aCC-BY-NC-ND 4.0 International license.

47 enhancers with fewer false positives. Overall, we demonstrate an optimized processing
48 framework for STARR-seq experiments can identify putative enhancers while
49 addressing potential confounders.

50 **Keywords**: STARR-seq, peak caller, enhancer, non-coding, regulatory element

51

52 Background

53 The transcription of eukaryotic genes is precisely coordinated by an interplay between
54 *cis*-regulatory elements. For example, enhancers and promoters serve as binding
55 platforms for transcription factors (TFs) and allow them to interact with each other via
56 three-dimensional looping of chromatin. Their interactions are often required to initiate
57 transcription [1,2]. Enhancers, which are often distant from the transcribed gene body
58 itself, play critical roles in the upregulation of gene transcription. Enhancers are cell-type
59 specific and can be epigenetically activated or silenced to modulate transcriptional
60 dynamics over the course of development. Enhancers can be found upstream or
61 downstream of genes, or even within introns [3–5]. They function independent of their
62 orientation, do not necessarily regulate the closest genes, and sometimes regulate
63 multiple genes at once [6,7]. In addition, several recent studies have demonstrated that
64 some promoters – termed E-promoters – may act as enhancers of distal genes [8,9].

65

66 Consensus sequences (or canonical sequences) have been identified at certain protein
67 binding sites, splice sites, and boundaries of protein-coding genes. However, there are
68 no known consensus sequences that characterize enhancer function, making it
69 challenging to identify enhancers based on sequence alone in an unbiased fashion. The

bioRxiv preprint doi: https://doi.org/10.1101/694869; this version posted May 5, 2020. The copyright holder for this preprint (which was not certified by peer review) is the author/funder, who has granted bioRxiv a license to display the preprint in perpetuity. It is made available under aCC-BY-NC-ND 4.0 International license.

70 non-coding territory occupies over 98% of the genome landscape, making the search
71 space very broad. Moreover, the activity of enhancers depends on the physiological
72 condition and epigenetic landscape of the cellular environment, complicating a fair
73 assessment of enhancer function.

74 Previously, putative regulatory elements were computationally predicted, indirectly, by
75 profiling DNA accessibility (using DNase-seq, FAIRE-seq, or ATAC-seq) as well as
76 histone modifications (ChIP-seq) that are linked to regulatory functions [10–12]. More
77 recently, researchers have developed high-throughput episomal (exogenous) reporter
78 assays to directly measure enhancer activity across the whole genome, specifically
79 massively parallel reporter assays (MPRA) [13,14] and self-transcribing active
80 regulatory region sequencing (STARR-seq) [15,16]. These assays allow for quantitative
81 assessment of enhancer activity in a high-throughput fashion.

82 In STARR-seq, candidate DNA fragments are cloned downstream of a reporter gene
83 into the 3′ untranslated region (UTR). After transfecting the plasmid pool into host cells,
84 one can measure the regulatory potential by high-throughput sequencing of the 3′ UTR
85 of the expressed reporter gene mRNA. These exogenous reporters enable accurate
86 and unbiased assessment of enhancer activity at the whole-genome level, independent
87 of chromatin context. Unlike MPRA – which utilizes barcodes – STARR-seq produces
88 self-transcribed RNA fragments that can be directly mapped onto the genome (we call
89 this STARR-seq output hereafter). The activities of enhancers are measured by
90 comparing the amount of RNA produced from the relative amount of genomic DNA in
91 the STARR-seq library (we call this STARR-seq input hereafter). STARR-seq has
92 several technical advantages over MPRA. Library construction is relatively simple

bioRxiv preprint doi: https://doi.org/10.1101/694869; this version posted May 5, 2020. The copyright holder for this preprint (which was not certified by peer review) is the author/funder, who has granted bioRxiv a license to display the preprint in perpetuity. It is made available under aCC-BY-NC-ND 4.0 International license.

93 because barcodes are not needed. In addition, candidate enhancers are cloned instead
94 of synthesized, allowing the assay to test extended sequence contexts (>500 bp) for
95 enhancer activity, which studies have shown to be critical for functional activity [17].
96 Importantly, STARR-seq can be scaled to the whole-genome level for unbiased
97 scanning of functional activities. However, scaling STARR-seq to the human genome is
98 still very challenging, primarily due to its massive size. A more complex genomic DNA
99 library, a higher sequencing depth, and increased transfection efficiency are required to
100 cover the whole human genome [16], which could ultimately introduce biases.
101 Furthermore, inserting a large fragment of DNA into the 3' UTR of the reporter gene
102 could inadvertently introduce regulatory sequences that might affect mRNA abundance
103 and stability, which could lead to both false positives and false negatives. MPRA is
104 more robust in this regard because the activity of each candidate enhancer is quantified
105 by multiple molecular barcodes associated with the fragment, making it less prone to
106 such artifacts than STARR-seq.
107 The processing of STARR-seq data is somewhat similar to that of ChIP-seq, where
108 protein-crosslinked DNA is immunoprecipitated and sequenced. A typical ChIP-seq
109 processing pipeline identifies genomic regions over-represented by sequencing tags in
110 a ChIP sample compared to a control sample. STARR-seq data is compatible with most
111 ChIP-seq peak callers. Hence, previous studies on STARR-seq have largely relied on
112 peak-calling software developed for ChIP-seq such as MACS2 [16,18,19]. However,
113 one must be cautious using ChIP-seq peak callers, at least without re-tuning the default
114 parameters optimized for processing TF ChIP-seq [20].

bioRxiv preprint doi: https://doi.org/10.1101/694869; this version posted May 5, 2020. The copyright holder for this preprint (which was not certified by peer review) is the author/funder, who has granted bioRxiv a license to display the preprint in perpetuity. It is made available under aCC-BY-NC-ND 4.0 International license.

115 In this paper, we describe key differences in the processing of STARR-seq versus
116 ChIP-seq data. Due to increased complexity of the genomic screening library and
117 sequencing depth requirements, STARR-seq coverage is highly non-uniform. This leads
118 to a lower signal-to-noise ratio than a typical ChIP-seq experiment and makes
119 estimating the background model more challenging, which could ultimately lead to false-
120 positive peaks. In addition, STARR-seq measures more of a continuous activity, similar
121 to quantification in RNA-seq, than a discrete binding event. Therefore, STARR-seq
122 peaks should be further evaluated using a notion of activity score. These differences
123 necessitate a unique approach to processing STARR-seq data.
124 We propose an algorithm optimized for processing and identifying functionally active
125 enhancers from STARR-seq data, which we call STARRPeaker. This approach
126 statistically models the basal level of transcription, accounting for potential confounding
127 factors, and accurately identifies reproducible enhancers. We applied our method to two
128 whole human STARR-seq datasets and evaluated its performance against previous
129 methods. We also compared an R package, BasicSTARRseq, developed to process
130 peaks from the first STARR-seq data [15], which models enrichment of sequencing
131 reads using a binomial distribution. We benchmarked our peak calls against known
132 human enhancers. Thus, our findings support that STARRPeaker will be a useful tool
133 for uniformly processing STARR-seq data.
134

135 ## Results and Discussion

136 ### Precise measurement of STARR-seq coverage

bioRxiv preprint doi: https://doi.org/10.1101/694869; this version posted May 5, 2020. The copyright holder for this preprint (which was not certified by peer review) is the author/funder, who has granted bioRxiv a license to display the preprint in perpetuity. It is made available under aCC-BY-NC-ND 4.0 International license.

137 We binned the genome using a sliding window of length, *l*, and step size, *s*. Based on
138 the average size of the STARR-seq library, we defined a 500 bp window length with a
139 100 bp step size to be the default parameter. Based on the generated genomic bins, we
140 calculated the coverage of both STARR-seq input and output mapped to each bin. For
141 calculating the sequence coverage, other peak callers and many visualization tools
142 commonly use the start position of the read [15,21,22]. However, given that the average
143 size of the fragments inserted into the STARR-seq libraries were approximately 500 bp,
144 we expected that the read coverage using the read start position may shift the estimate
145 of the summit of signal and dilute the enrichment. Some peak callers have used read
146 densities of forward and reverse strands separately to overcome this issue [23,24]. To
147 precisely measure the coverage of STARR-seq input and output, we first inferred the
148 size of the fragment insert from paired-end reads and used the center of the fragment
149 insert, instead of start position of the read, to calculate coverage. For inferring the size
150 of the fragment insert, we first strictly filtered out reads that were not properly paired and
151 chimeric. Chimeric alignments are reads that cannot be linearly aligned to a reference
152 genome, implying a potential discrepancy between the sequenced genome and the
153 reference genome and indicative of a structural variation or a PCR artifact [25]. We also
154 filtered out read pairs that had a fragment insert size greater than l_{max} and less than
155 l_{min}. By default, we filtered out fragment insert sizes less than 200 bp and greater than
156 1,000 bp. After filtering out spurious read-pairs, we estimated the center of the fragment
157 insert and counted the fragment depth for each genomic bin. To assess the benefit of
158 using fragment-based coverage, we compared the coverage calculated using the center
159 of fragment insert to an alternate model using the start position of the sequencing read.

bioRxiv preprint doi: https://doi.org/10.1101/694869; this version posted May 5, 2020. The copyright holder for this preprint (which was not certified by peer review) is the author/funder, who has granted bioRxiv a license to display the preprint in perpetuity. It is made available under aCC-BY-NC-ND 4.0 International license.

160 We found that the position of the peaks shifted up approximately 200 bp when we used
161 the alternate model (Figure 1A, Supplementary Figure 1A). Such a shift caused by the
162 read-based coverage could lead to the omission of TF binding sites located at the
163 boundary. Moreover, we observed that the read-based coverage diluted the overall
164 STARR-seq signal; as a result, peaks calculated based on the alternate model had
165 lower fold enrichment and were less confident and broader in size (Figure 1B-D,
166 Supplementary Figure 1B-D). Overall, the fragment-based coverage offered more
167 concentrated and robust peak signal compared to the read-based coverage counting
168 scheme. The benefit of using the center of the fragment is highlighted in Figure 1E,
169 where we find more concise and precise peak with a higher fold enrichment using
170 fragment-based coverage.
171

172 **Controlling for potential systemic bias in the STARR-seq assay**

173 To unbiasedly test for the regulatory activity, a model needs to control for potential
174 systemic biases inherent to generating STARR-seq data. STARR-seq measures the
175 ratio of transcribed RNA to DNA for a given test region and determines whether the test
176 region can facilitate transcription at a higher rate than the basal level. This is based on
177 the assumption that (1) the basal transcriptional level stays relatively constant across
178 the genome and (2) the transcriptional rate is a reflection of the regulatory activity of the
179 DNA insert. However, these assumptions may not always be true, and one needs to
180 consider potential systemic biases that can interfere with the quantification of regulatory
181 activity when analyzing the data.

bioRxiv preprint doi: https://doi.org/10.1101/694869; this version posted May 5, 2020. The copyright holder for this preprint (which was not certified by peer review) is the author/funder, who has granted bioRxiv a license to display the preprint in perpetuity. It is made available under aCC-BY-NC-ND 4.0 International license.

182 We next tested whether potential sequencing biases and other covariates confounded
183 STARR-seq readouts (Figure 2). We found that STARR-seq RNA coverage was
184 significantly correlated with GC content (PCC 0.61; P-val 1E-299) and mappability (PCC
185 0.45; P-val 2.9E-148). This could be attributed to intrinsic sequencing biases in library
186 preparation. A genome-wide reporter library is made from randomly sheared genomic
187 DNA, but DNA fragmentation is often non-random [26]. Studies also have suggested
188 that epigenetic mechanisms and CpG methylation may influence fragmentation [27].
189 Furthermore, the isolated polyadenylated RNAs are reverse transcribed and PCR
190 amplified before sequencing, and this process can further confound the sequenced
191 candidate fragments.
192 Notably, we found that STARR-seq coverage was also significantly confounded by RNA
193 thermodynamic stability (PCC -0.55; P-val 0). Unlike ChIP-seq, where both the
194 experiment and input controls derive from the same DNA origin, STARR-seq
195 experiments measure the regulatory potential from the abundance of transcribed RNA,
196 which adds a layer of complexity. For example, RNA structure and co-transcriptional
197 folding might potentially influence the readout of STARR-seq experiments [28]. Single-
198 stranded RNA starts to fold upon transcription and the resulting RNA structure might
199 influence the measurement of regulatory activity. Previously, researchers suggested a
200 potential linkage between RNA secondary structure and transcriptional regulation [29].
201 In addition, the resulting transcribed RNA undergoes a series of post-transcriptional
202 regulation, and RNA stability might play a critical role. Moreover, previous reports have
203 shown that the degradation rates – the main determinant of cellular RNA levels [30] –

bioRxiv preprint doi: https://doi.org/10.1101/694869; this version posted May 5, 2020. The copyright holder for this preprint (which was not certified by peer review) is the author/funder, who has granted bioRxiv a license to display the preprint in perpetuity. It is made available under aCC-BY-NC-ND 4.0 International license.

204 vary significantly across the genome and that RNA stability correlates with functionality
205 [31,32].
206 Based on these findings, we built a regression-based model that accounts for various
207 confounding variables of test sequence fragments to unbiasedly identify potential
208 enhancer regions from STARR-seq data. Note that many of the covariates have
209 appreciable correlation with each other. However, we did find, using stepwise forward
210 selection, that each of them contributes substantially and independently to the model fit
211 as assessed by Akaike information criterion (AIC) and Bayesian information criterion
212 (BIC) (Supplementary Figure 2).
213

214 **Accurate modelling of STARR-seq using negative binomial regression**

215 To model the fragment coverage data from STARR-seq using discrete probability
216 distribution, we assumed that each genomic bin is independent and identically
217 distributed, as specified in the Bernoulli trials [33]. That is, each test fragment can only
218 map to a single fixed-length bin. Therefore, we only considered a non-overlapping
219 subset of bins for modeling and fitting the distribution. We also excluded bins not
220 covered by any genomic input or those in which the normalized input coverage was less
221 than a minimum quantile t_{min}, since these regions do not have sufficient power to detect
222 enrichment. We selected the bin size and the minimum coverage based on the
223 experimental design of STARR-seq. We simulated and fitted various discrete probability
224 distributions to STARR-seq output coverage. We observed that the STARR-seq output
225 coverage data was overdispersed and fit the best with a negative binomial distribution

bioRxiv preprint doi: https://doi.org/10.1101/694869; this version posted May 5, 2020. The copyright holder for this preprint (which was not certified by peer review) is the author/funder, who has granted bioRxiv a license to display the preprint in perpetuity. It is made available under aCC-BY-NC-ND 4.0 International license.

226 (Figure 3A). Moreover, a Q-Q plot of simulated coverage further demonstrated that the
227 negative binomial model provides the best fit for the data (Figure 3B).
228 We observed a slight negative enrichment in the STARR-seq output coverage,
229 suggesting that some candidate fragments can repress the basal transcriptional activity.
230 However, these regions may contain sequences that can destabilize mRNAs. Therefore,
231 additional experiments are necessary to demonstrate that STARR-seq can reliably
232 detect silencers. In the meantime, we suggest opting for a system specifically designed
233 for identifying silencers for this task [34].
234

235 **Peak-calling algorithm**

236 To accurately model the ratio of STARR-seq output fragment coverage (RNA) to input
237 fragment coverage (DNA) while controlling for potential confounding factors, we applied
238 a negative binomial regression. The overview of our model is outlined in Figure 4. Our
239 model starts by fitting an analytical distribution to the observed fragment coverage
240 across fixed non-overlapping genomic bins. In doing so, we use covariates to model
241 expected counts in the form of multiple regression. Subsequently, once a model is fitted,
242 we evaluate the likelihood of obtaining the observed fragment counts and assign p-
243 values using the null negative binomial distribution. In this testing phase, we use flexible
244 genomic bins with a sliding window in order to find enrichment peaks at a higher
245 resolution. Genomic bins with significant enrichments are selected based on their
246 adjusted p-values using multiple testing correction. Finally, peak locations are fine-tuned
247 to the summit of the direct fragment coverage. Note that the adjusted p-value should be

bioRxiv preprint doi: https://doi.org/10.1101/694869; this version posted May 5, 2020. The copyright holder for this preprint (which was not certified by peer review) is the author/funder, who has granted bioRxiv a license to display the preprint in perpetuity. It is made available under aCC-BY-NC-ND 4.0 International license.

248 regarded as the likelihood of a candidate region being an enhancer while the fold
249 enrichment can be directly interpreted as a quantitative measure of enhancer activity.
250
251 Let Y be a vector of STARR-seq output (RNA) coverage, then y_i for $1 \leq i \leq n$ denotes
252 the number of RNA fragments from a STARR-seq experiment mapped to the i-th bin
253 from the total of n genomic bins. Let t_i be the number of input library fragments (DNA)
254 mapped to the i-th bin. We define X to be the matrix of covariates, where $\vec{x_i}$ is the vector
255 of covariates corresponding to the i-th bin and x_{ij} is the j-th covariate for the i-th bin.
256
257 *Negative binomial distribution*
258 A negative binomial distribution, which arises from a Gamma-Poisson mixture, can be
259 parametrized as follows [35–37] (see Methods for derivation).
260

$$f_Y(y_i|\mu_i,\theta) = \frac{\Gamma(y_i+\theta)}{\Gamma(y_i+1)\cdot\Gamma(\theta)}\cdot\left(\frac{\theta}{\theta+\mu_i}\right)^{\theta}\cdot\left(\frac{\mu_i}{\theta+\mu_i}\right)^{y_i} \quad (1)$$

261
262 A negative binomial is a generalization of a Poisson regression that allows the variance
263 to be different from the mean, shaped by the dispersion parameter θ. There are two
264 alternative forms of parametrization for a negative binomial – NB1 and NB2 – which
265 were first introduced by Cameron and Trivedi [36]. The difference between NB1 and
266 NB2 is in the conditional variance of y_i. Assuming y_i has mean λ_i, the general variance
267 function follows the form $\omega_i = \lambda_i + \alpha {\lambda_i}^p$, where α is a scalar parameter. NB1 uses $p = 1$,
268 whereas NB2 uses the quadratic form of variance with $p = 2$. We use the most common

bioRxiv preprint doi: https://doi.org/10.1101/694869; this version posted May 5, 2020. The copyright holder for this preprint (which was not certified by peer review) is the author/funder, who has granted bioRxiv a license to display the preprint in perpetuity. It is made available under aCC-BY-NC-ND 4.0 International license.

269 implementation of the negative binomial, NB2, hereafter. The variance for the NB2

270 model is given as

271

$$\sigma^2 = \mu + \frac{\mu^2}{\theta} \quad \text{(Error! Bookmark not defined.)}$$

272

273 We assume that the majority of genomic bins will have a basal level of transcription, the

274 expected fragment counts at each i-th bin, $E(y_i)$, represents the mean incidence, μ_i,

275 and the count of RNA fragments Y follows the traditional negative binomial (NB2)

276 distribution.

277

$$E(y_i) = \mu_i$$
$$Y \sim NB(\mu, \theta) \tag{2}$$

278

279 <u>*Negative binomial regression model*</u>

280 The regression term for the expected RNA fragment count can be expressed in terms of

281 a linear combination of explanatory variables, a set of m covariates ($\vec{x}$). We use the

282 input library variable t_i as one covariate. For simplicity, we denote t_i as x_{0i} hereafter.

283

$$\ln \mu_i = \beta_0 x_{0i} + \beta_1 x_{1i} + \cdots + \beta_m x_{mi}$$
$$\mu_i = \exp(\beta_0 x_{0i} + \beta_1 x_{1i} + \cdots + \beta_m x_{mi}) \tag{3}$$
$$\mu_i = \exp\left(\vec{x_i}^{\intercal} \beta\right)$$

284

bioRxiv preprint doi: https://doi.org/10.1101/694869; this version posted May 5, 2020. The copyright holder for this preprint (which was not certified by peer review) is the author/funder, who has granted bioRxiv a license to display the preprint in perpetuity. It is made available under aCC-BY-NC-ND 4.0 International license.

285 Alternatively, instead of using the input library variable t_i as one covariate, we can
286 directly use it as an offset variable. Generally, a fractional observation cannot be
287 modeled using discrete probability. However, an offset variable in a generalized linear
288 model can be used to correct the response term to behave like a fraction. One
289 advantage of using the input variable as an “exposure” to the RNA output coverage is
290 that it allows us to directly model the basal transcription rate (the ratio of RNA to DNA)
291 as a rate response variable. More details on this alternative parametrization are
292 included in the Methods section. In our STARRPeaker model, we used four covariates;
293 fragment coverage of input genomic libraries, GC content, mappability, and the
294 thermodynamic stability of genomic libraries.
295
296 *Maximum-likelihood estimation*
297 We fit the model and estimate regression coefficients using the maximum likelihood
298 method, where log-likelihood function is shown as follows.
299

$$\mathcal{L}_{NB}(\mu|y,\theta) = \sum_{i=1}^{n} y_i \ln\left(\frac{\mu_i}{\theta+\mu_i}\right) + \theta \ln\left(\frac{\theta}{\theta+\mu_i}\right) + \ln\left(\frac{\Gamma(y_i+\theta)}{\Gamma(y_i+1)\cdot\Gamma(\theta)}\right) \quad \text{(Error! Bookmark not defined.)}$$

300
301 Substituting μ_i with the regression term, the log-likelihood function can be parametrized
302 in terms of regression coefficients, β.
303

bioRxiv preprint doi: https://doi.org/10.1101/694869; this version posted May 5, 2020. The copyright holder for this preprint (which was not certified by peer review) is the author/funder, who has granted bioRxiv a license to display the preprint in perpetuity. It is made available under aCC-BY-NC-ND 4.0 International license.

$$\mathcal{L}_{NB}(\beta|y,\theta) = \sum_{i=1}^{n} y_i \ln\left(\frac{e^{\vec{x_i}^\intercal \beta}}{\theta + e^{\vec{x_i}^\intercal \beta}}\right) + \theta \ln\left(\frac{\theta}{\theta + e^{\vec{x_i}^\intercal \beta}}\right) + \ln\left(\frac{\Gamma(y_i+\theta)}{\Gamma(y_i+1)\cdot\Gamma(\theta)}\right) \quad \text{(Error! Bookmark not defined.)}$$

304

305 We can determine the maximum likelihood estimates of the model parameters by
306 setting the first derivative of the log-likelihood with respect to β, the gradient, to zero,
307 and there is no analytical solution for $\hat{\beta}$. Numerically, we iteratively solve for the
308 regression coefficients β and the dispersion parameter θ, alternatively, until both
309 parameters converge.

310

311 *Estimation of P-value*

312 The P-value is defined as the probability of observing equal or more extreme value than
313 the observed value at the i-th bin, y_i, under the null hypothesis.

314

$$P\text{–}value_i = \Pr(Y \geq y_i|H) \quad (4)$$

315

316 As defined earlier, we assume the random variable Y comes from a negative binomial
317 distribution with the fitted mean at the i-th bin, μ_i, as the expected value, and θ as the
318 dispersion parameter. Then, we can estimate the P-value from the cumulative
319 distribution function CDF, which is the sum of the probability mass function f_Y from 0 to
320 $y_i - 1$.

321

bioRxiv preprint doi: https://doi.org/10.1101/694869; this version posted May 5, 2020. The copyright holder for this preprint (which was not certified by peer review) is the author/funder, who has granted bioRxiv a license to display the preprint in perpetuity. It is made available under aCC-BY-NC-ND 4.0 International license.

$$\Pr(Y \geq y_i|H) = 1 - CDF(y_i - 1) = 1 - \sum_{k=0}^{y_i-1} f_Y(k|\mu_i, \theta) \quad (5)$$

322

323 Substituting (1) gives

324

$$P\text{-}value_i = 1 - \sum_{k=0}^{y_i-1} \frac{\Gamma(k+\theta)}{\Gamma(k+1)\cdot\Gamma(\theta)} \cdot \left(\frac{\theta}{\theta+\mu_i}\right)^{\theta} \cdot \left(\frac{\mu_i}{\theta+\mu_i}\right)^{k} \quad (6)$$

325

326 Finally, we calculate the false discovery rate using *Benjamini & Hochberg* method [38].

327

328 **Application of STARRPeaker**

329 We applied STARRPeaker to two whole human genome STARR-seq experiments,
330 K562 and HepG2, utilizing origin of replication (ORI)-based plasmids [39]. Based on
331 peaks identified from these datasets, we evaluated the quality and characteristics of the
332 identified enhancers as well as the performance of the peak caller by comparing to
333 external enhancer resources.

334

335 *Initial evaluation of STARRPeaker enhancers*

336 We processed two biological replicates from each cell type independently and assessed
337 the correlation between each pair. Overall, we observed high correlation between two
338 replicates (PCC=0.99 for both HepG2 and K562; see Supplementary Figure 3). By
339 intersecting peaks from two replicates, we identified 32,929 and 20,471 reproducible
340 candidate enhancers from HepG2 and K562, respectively (Supplementary Table S1).

bioRxiv preprint doi: https://doi.org/10.1101/694869; this version posted May 5, 2020. The copyright holder for this preprint (which was not certified by peer review) is the author/funder, who has granted bioRxiv a license to display the preprint in perpetuity. It is made available under aCC-BY-NC-ND 4.0 International license.

341 Although the total number of peaks varied between HepG2 and K562, we observed a
342 comparable number of peaks within the accessible region of the genome. We found
343 12,019 (36.34%) and 11,420 (55.57%) candidate enhancers from HepG2 and K562,
344 respectively, within the open chromatin defined by ENCODE DNase-seq hotspots.
345 Consistent with previous findings [39], a substantial fraction of candidate enhancers was
346 epigenetically silenced at the chromatin level. However, as demonstrated previously
347 using a histone deacetylase inhibitor (HDAC) [16], these poised enhancers can become
348 functional under a more transcriptionally permissive environment. Therefore, episomal
349 reporter assays like STARR-seq have the unique advantage of detecting potential
350 enhancer activity independent from chromatin context. We would like to note that it is
351 important to identify poised enhancers located in heterochromatic regions of the
352 genome, which could become functional during developmental or pathological time
353 courses.
354
355 *Assessment of robustness and reproducibility of the method*
356 A reliable peak-calling method should be able to identify peaks from suboptimal
357 datasets. To evaluate the robustness of STARRPeaker, we used subsets of the whole-
358 genome STARR-seq library to call peaks and compared the results. We subsampled
359 randomly at various rates from 20 to 80% of the total dataset and compared the quality
360 of peaks. We found that STARRPeaker was able to reliably identify the peaks using
361 approximately 60% of the original sequencing library (Supplementary Figure 4).
362 However, the quality of the peak calls started to deteriorate when 40% or less were
363 used.

bioRxiv preprint doi: https://doi.org/10.1101/694869; this version posted May 5, 2020. The copyright holder for this preprint (which was not certified by peer review) is the author/funder, who has granted bioRxiv a license to display the preprint in perpetuity. It is made available under aCC-BY-NC-ND 4.0 International license.

364

365 *Evaluation of potential orientation bias in candidate enhancers*

366 In general, enhancers are thought to function independent of orientation [40]. However,
367 the fragment counts in one orientation could be skewed over the other due to
368 orientation-specific activities, PCR, or sequencing artifacts. To test for potential
369 orientation-based biases, we ran a binomial test on the candidate enhancers we
370 identified. We observed a small fraction of candidate enhancers showing strand bias
371 [3.19% for HepG2 rep1 (n=1,605); 3.76% for HepG2 rep2 (n=1,991); 7.77% for K562
372 rep1 (n=2,347); 5.25% for K562 rep2 (n=2,195); FDR ≤ 0.01] (Supplementary Figure 5).
373 Less than one third of the enhancers (n=690) showed strand-specific activity in both
374 replicates. Thus, we conclude that there is insufficient evidence to show that orientation-
375 dependent biases are present in our STARR-seq data. Furthermore, this finding
376 provides further support that enhancers function independent of orientation.

377

378 *Performance comparison to other peak-calling algorithms*

379 We evaluated the performance of STARRPeaker by comparing it to previously used
380 methods, namely BasicSTARRseq and MACS2.
381 First, we qualitatively assessed the peak-calling algorithms using a simulated dataset
382 where the ground truth exists. We created a STARR-seq dataset that consists of four
383 spike-in controls (hybrid of DNA input library and RNA output library of known specific
384 location). All three methods successfully identified the four control peaks with high
385 confidence (Supplementary Figure 6). However, we noticed that BasicSTARRseq peaks
386 were fragmented due to its limitation of fixed peak size. Moreover, the peaks were

bioRxiv preprint doi: https://doi.org/10.1101/694869; this version posted May 5, 2020. The copyright holder for this preprint (which was not certified by peer review) is the author/funder, who has granted bioRxiv a license to display the preprint in perpetuity. It is made available under aCC-BY-NC-ND 4.0 International license.

387 shifted toward the enrichment of sequencing reads. Furthermore, BasicSTARRseq
388 identified a false-positive peak, and as a result, identified a total of eight regions instead
389 of four.
390 Second, we quantitatively assessed the peak-calling algorithms using the whole human
391 genome STARR-seq dataset. After uniformly calling peaks from each method using the
392 recommended default settings, we evaluated the quality of the candidate enhancers
393 identified. We found that both BasicSTARRseq and MACS2 called significantly more
394 peaks (4 to 20-fold higher) than STARRPeaker (Supplementary Table S4). While it is
395 uncertain how many true enhancers were present in each sample, we had to ensure
396 that we made a fair comparison across different methods due to the tradeoff between
397 sensitivity and specificity. An increase in sensitivity is generally achieved at the expense
398 of a decrease in specificity, as described in receiver operating characteristic curves. In
399 our context, a method having higher specificity suffers from having less overlap with
400 open chromatin and previously identified enhancers from other assays. Therefore, we
401 used a uniform P-value threshold of 0.001 and subsampled the peaks before the
402 comparison. After uniformly processing the dataset using each method, we measured
403 the level of epigenetic profile enrichment around the peaks. We observed higher
404 enrichment of DNase-hypersensitive sites, as well as more distinct double-peak
405 patterns of H3K27ac and H3K4me1, using STARRPeaker compared to
406 BasicSTARRseq or MACS2 (Figure 5, Supplementary Figure 7). Furthermore,
407 STARRPeaker peaks had significantly higher enrichment of TF binding events (based
408 on the number of TF ChIP-seq binding sites) compared to the peaks identified using
409 other methods.

bioRxiv preprint doi: https://doi.org/10.1101/694869; this version posted May 5, 2020. The copyright holder for this preprint (which was not certified by peer review) is the author/funder, who has granted bioRxiv a license to display the preprint in perpetuity. It is made available under aCC-BY-NC-ND 4.0 International license.

410

411 *Comparison to previously characterized enhancers*

412 First, we compared the peaks identified by STARRPeaker to previously characterized
413 enhancers from HepG2 or K562 cell lines by CAGE [41], MPRA [17,42], and STARR-
414 seq [19] (Figure 6, Supplementary Table S2). Overall, we observed a higher fraction of
415 STARRPeaker peaks overlapping with external datasets compare to other methods.
416 Moreover, we found higher overlaps when peaks from both replicates were merged, due
417 to fewer but more precise candidate enhancers from merging replicates. However, we
418 noticed reduced agreement across different types of enhancer assays. Low overlap
419 between assays may arise from different formats or layouts of reporter plasmids, such
420 as differing enhancer cloning sites or promoters, or differences in the complexity of the
421 screening library. Furthermore, CAGE is an entirely different assay from episomal
422 reporter assays like MPRA and STARR-seq, with enhancers defined based on
423 bidirectional transcripts originating from an eRNA.
424 Second, we examined the nine distal enhancers from the GATA1 and MYC loci
425 characterized in-depth by CRISPRi tiling screen (Supplementary Figure 8). We found
426 that STARRPeaker accurately called peaks for 6 of 9 enhancers from both replicates.
427 For the remaining three regions, we observed insufficient enrichment of STARR-seq
428 output and, therefore, we concluded that this is not a shortcoming of the peak caller.
429

430 *Application to external STARR-seq datasets*

431 To ensure that STARRPeaker can be generally applied to different variants of STARR-
432 seq assays, we tested STARRPeaker on previously published STARR-seq datasets.

bioRxiv preprint doi: https://doi.org/10.1101/694869; this version posted May 5, 2020. The copyright holder for this preprint (which was not certified by peer review) is the author/funder, who has granted bioRxiv a license to display the preprint in perpetuity. It is made available under aCC-BY-NC-ND 4.0 International license.

433 First, we applied STARRPeaker to the whole-genome ORI-STARR-seq dataset on
434 HeLa-S3 [39] and assessed the quality of the peaks identified. Consistent with the
435 previous claim that IFN-I signaling may induce false-positive enhancers, we identified
436 more peaks in untreated HeLa-S3 samples (n=28,381) compared to inhibitor-treated
437 samples (n=16,150). Furthermore, peaks from untreated samples had lower enrichment
438 of chromatin accessibility (DNase-seq) than those from inhibitor-treated samples,
439 supporting that TBK1/IKK/PKR inhibition reduces false-positive enhancer signals related
440 to IFN-I signaling (Supplementary Figure 9A). Moreover, STARRPeaker covered 77.5%
441 (n=7,451) of published peaks, which were called using BasicSTARRseq and then
442 further shortlisted using a stringent threshold (P-value 1E-5 with corrected enrichment ≥
443 4). Furthermore, STARRPeaker found 6,540 additional peaks from a HeLa-S3 sample
444 that was highly enriched with chromatin accessibility signals (Supplementary Figure 9B).
445 Second, we tested if STARRPeaker can be reliably applied to captured STARR-seq
446 datasets (Cap-STARR-seq). We applied STARRPeaker to a previously characterized
447 GM12878 STARR-seq dataset based on an ATAC-seq-capture technique called HiDRA
448 [43] and compared its performance with published results. The HiDRA dataset was
449 reported to have ~65,000 regions with enhancer function. In the STARRPeaker run, we
450 identified only 20,852 regions with significant enhancer activities from the five replicates
451 they produced. Approximately 73.6% of peaks overlapped with the published results
452 (n=15,347). While it is debatable to claim that one method is superior to the other, this
453 result demonstrates that STARRPeaker can be reliably used against the Cap-STARR-
454 seq dataset.

bioRxiv preprint doi: https://doi.org/10.1101/694869; this version posted May 5, 2020. The copyright holder for this preprint (which was not certified by peer review) is the author/funder, who has granted bioRxiv a license to display the preprint in perpetuity. It is made available under aCC-BY-NC-ND 4.0 International license.

455 Third, we further evaluated the performance of the peak-calling methods by applying
456 STARRPeaker and two other peak-calling methods to another published Cap-STARR-
457 seq dataset [19]. The dataset covers approximately 91% of the surrounding 3 Mb of the
458 MYC locus. Consistent with the earlier analysis, we observed that STARRPeaker is
459 highly specific and identifies fewer candidate enhancers (n=26) compared to the other
460 methods (BasicSTARRseq n=223; MACS2 n=136). Furthermore, a four-way
461 comparison (STARRPeaker, BasicSTARRseq, MACS2, and published peaks) showed
462 that all of the STARRPeaker peaks overlapped with peaks from other methods but not
463 the other way around (Supplementary Figure 10). These results indicate that
464 STARRPeaker is more robust and reliable at identifying reproducible candidate
465 enhancers from various STARR-seq datasets than previous methods.
466

467 ## Conclusions

468 In summary, we developed a reliable peak-calling analysis pipeline named
469 STARRPeaker that is optimized for large-scale STARR-seq experiments. To illustrate
470 the utility of our method, we applied it to two whole human genome STARR-seq
471 datasets from K562 and HepG2 cell lines, utilizing ORI-based plasmids.
472 STARRPeaker has several key improvements over previous approaches including (1)
473 precise and efficient calculation of fragment coverage; (2) accurate modeling of the
474 basal transcription rate using negative binomial regression; and (3) accounting for
475 potential confounding factors, such as GC content, mappability, and the thermodynamic
476 stability of genomic libraries. We demonstrate the superiority of our method over

bioRxiv preprint doi: https://doi.org/10.1101/694869; this version posted May 5, 2020. The copyright holder for this preprint (which was not certified by peer review) is the author/funder, who has granted bioRxiv a license to display the preprint in perpetuity. It is made available under aCC-BY-NC-ND 4.0 International license.

477 previously used peak callers, supported by strong enrichment of epigenetic marks
478 relevant to enhancers and overlap with previously known enhancers.
479
480 To fully understand how noncoding regulatory elements can modulate transcriptional
481 programs in human, STARR-seq active regions must be further characterized and
482 validated within different cellular contexts. For example, recent applications of CRISPR-
483 dCas9 to genome editing have allowed researchers to epigenetically perturb and test
484 these elements in their native genomic context [44,45]. The next step for CRISPR-
485 based functional screens is to overcome the current limitation of small scale by
486 leveraging barcodes and single-cell sequencing technology [46]. In the meantime, we
487 envision that the STARRPeaker framework could be utilized to detect and quantify
488 enhancers at the whole-genome level, thereby aiding in prioritizing candidate regions in
489 an unbiased fashion to maximize functional characterization efforts.
490

491 ## Methods

492 ### Cell culture

493 We cultured K562 cells (ATCC) in IMDM (Gibco #12440) supplemented with 10% fetal
494 bovine serum (FBS) and 1% pen/strep and maintained in a humidified chamber at 37°C
495 with 5% CO_2. We cultured HepG2 cells (ATCC) in EMEM (ATCC #30-2003)
496 supplemented with 10% FBS and 1% pen/strep, maintained in a humidified chamber at
497 37°C with 5% CO_2.
498

499 ### Generating an ORI-STARR-seq input plasmid library

bioRxiv preprint doi: https://doi.org/10.1101/694869; this version posted May 5, 2020. The copyright holder for this preprint (which was not certified by peer review) is the author/funder, who has granted bioRxiv a license to display the preprint in perpetuity. It is made available under aCC-BY-NC-ND 4.0 International license.

500 We sonicated human male genomic DNA (Promega #G1471) using a Covaris S220
501 sonicator (duty factor – 5%; cycle per burst – 200; 40 sec) and ran it on a 0.8% agarose
502 gel to size-select 500 bp fragments. After gel purification using a MinElute Gel
503 Extraction kit (Qiagen), we end-repaired, ligated custom adaptors, and PCR-amplified
504 DNA fragments using Q5 Hot Start High-Fidelity DNA polymerase (NEB) (98°C for 30
505 sec; 10 cycles of 98°C for 10 sec, 65°C for 30 sec, and 72°C for 30 sec; 72°C for 2 min)
506 to add homology arms for Gibson assembly cloning.
507 We used AgeI-HF (NEB) and SalI-HF (NEB) to linearize the hSTARR-seq_ORI plasmid
508 (gift from Alexander Stark; Addgene plasmid #99296) and cloned the PCR products into
509 the vector using Gibson Assembly Master Mix (NEB); we set up 60 replicate reactions
510 to maintain complexity. We purified the assembly reactions using SPRI beads
511 (Beckman Coulter), dialyzed them using Slide-A-Lyzer MINI dialysis devices
512 (ThermoScientific), and concentrated them using an Amicon Ultra-0.5 device (Amicon).
513 We transformed the reaction into MegaX DH10BTM T1 electrocompetent cells (Thermo
514 Fisher Scientific) (with 25 replicate transformations to maintain complexity) and let them
515 grow in 12.5L LB-Amp medium until they reached an optical density of ~1.0. We
516 extracted the plasmids using a Plasmid Gigaprep Kit (Qiagen) and dialyzed the plasmid
517 prep using Slide-A-Lyzer MINI dialysis devices before electroporation.
518

519 **Electroporation-mediated transfection of ORI-STARR-seq input plasmid library**
520 **into K562 and HepG2 cell lines**

521 We electroporated the ORI-STARR-seq library using an AgilePulse Max (Harvard
522 Apparatus) and generated two biological replicates for each cell line. For K562 cells, we

bioRxiv preprint doi: https://doi.org/10.1101/694869; this version posted May 5, 2020. The copyright holder for this preprint (which was not certified by peer review) is the author/funder, who has granted bioRxiv a license to display the preprint in perpetuity. It is made available under aCC-BY-NC-ND 4.0 International license.

523 electroporated 5.6 mg of input plasmid library into 700 million cells per biological
524 replicate by delivering three 500 V pulses (1 ms duration with a 20 ms interval). For
525 HepG2 cells, we electroporated 8 mg of input plasmid library into one billion cells in one
526 replicate, and 5.6 mg into 700 million cells in another replicate by delivering three 300 V
527 pulses (5 ms duration with a 20 ms interval).
528

529 **Generation of an Illumina sequencing library**

530 *Output RNA library*: We harvested cells 24 hr after electroporation, and extracted total
531 RNA using an RNeasy Maxi kit (Qiagen). We further isolated polyA-plus mRNA using
532 Dynabeads® Oligo (dT) kit (ThermoFisher Scientific), treated it with TURBO DNase
533 (Invitrogen), and purified the reaction using an RNeasy MinElute Kit (Qiagen). We
534 synthesized cDNA using SuperScript III (ThermoFisher Scientific) with a custom primer
535 that specifically recognizes mRNAs that had been transcribed from the ORI-STARR-seq
536 library. After reverse transcription, we treated the reactions with a cocktail of RNase A
537 and RNase T1 (ThermoFisher Scientific). We split cDNA samples into 160 replicate
538 sub-reactions, and PCR-amplified each sub-reaction with a primer with a unique index
539 (helping to identify PCR duplicates) using Q5 Hot Start High-Fidelity DNA polymerase
540 (NEB) with the following program: 98°C for 30 s; cycles of 98°C for 10 s, 65°C for 30 s,
541 72°C for 30 s (until they reached mid-log amplification phase; we cycled 18 cycles for
542 K562 Rep.1; 16 cycles for K562 Rep. 2; 18 cycles for HepG2 Rep. 1; and 15 cycles for
543 HepG2 Rep2); 72°C for 2 min). After PCR, we re-combined all sub-reactions into one
544 and purified it with Agencourt Beads. We generated 100 bp paired-end reads for each

bioRxiv preprint doi: https://doi.org/10.1101/694869; this version posted May 5, 2020. The copyright holder for this preprint (which was not certified by peer review) is the author/funder, who has granted bioRxiv a license to display the preprint in perpetuity. It is made available under aCC-BY-NC-ND 4.0 International license.

545 biological replicate on an Illumina Hiseq4000 at the University of Chicago Genome
546 Facility.
547 *Input DNA library*: We PCR-amplified a total of 200 ng of input plasmid library (in 16
548 replicate reactions) using Q5 Hot Start High-Fidelity DNA polymerase (NEB) with the
549 following program: 98°C for 30 s; 4 cycles of 98°C for 10 s, 65°C for 30 s, and 72°C for
550 20 s; 8 cycles of 98°C for 10 s and 72°C for 50 s; 72°C for 2 min). After PCR, we
551 combined all products into one and purified it with Agencourt Beads. We generated 100
552 bp paired-end reads on an Illumina Hiseq4000 at the University of Chicago Genome
553 Facility.
554

555 **Sequencing and preprocessing**

556 For each of 160 replicates, paired-end sequencing reads were aligned to the human
557 reference genome GRCh38 downloaded from the ENCODE portal (ENCSR425FOI)
558 using BWA-mem (v0.7.17). Alignments were filtered against unmapped, secondary
559 alignments, mapping quality score less than 30, and PCR duplicates using SAMtools
560 (v1.9) and Picard (v2.9.0). All of the replicates were pooled and sorted for downstream
561 analysis.
562

563 **Negative binomial distribution**

564 A negative binomial distribution, which arises from Gamma-Poisson mixture, can be
565 parametrized for y>=0 as follows.
566

$$Pr(Y = y_i|\mu_i, \theta) = f_Y(y_i; \mu_i, \theta) = \binom{y_i + \theta - 1}{y_i} \cdot \left(\frac{\theta}{\theta + \mu_i}\right)^{\theta} \cdot \left(\frac{\mu_i}{\theta + \mu_i}\right)^{y_i}$$

bioRxiv preprint doi: https://doi.org/10.1101/694869; this version posted May 5, 2020. The copyright holder for this preprint (which was not certified by peer review) is the author/funder, who has granted bioRxiv a license to display the preprint in perpetuity. It is made available under aCC-BY-NC-ND 4.0 International license.

567 where

$$\binom{y_i + \theta - 1}{y_i} = \frac{\Gamma(y_i + \theta)}{y_i! \cdot \Gamma(\theta)} = \frac{\Gamma(y_i + \theta)}{\Gamma(y_i + 1) \cdot \Gamma(\theta)}$$

568

569 Substituting gives:

$$f_Y(y_i; \mu_i, \theta) = \frac{\Gamma(y_i + \theta)}{\Gamma(y_i + 1) \cdot \Gamma(\theta)} \cdot \left(\frac{\theta}{\theta + \mu_i}\right)^{\theta} \cdot \left(\frac{\mu_i}{\theta + \mu_i}\right)^{y_i}$$

570

571 Rearranging gives:

572

$$f_Y(y_i; \mu_i, \theta) = \frac{\Gamma(y_i + \theta)}{\Gamma(y_i + 1) \cdot \Gamma(\theta)} \cdot \left(\frac{1}{1 + \frac{\mu_i}{\theta}}\right)^{\theta} \cdot \left(\frac{\frac{\mu_i}{\theta}}{1 + \frac{\mu_i}{\theta}}\right)^{y_i}$$

$$f_Y(y_i; \theta, \mu_i) = \frac{\Gamma(y_i + \theta)}{\Gamma(y_i + 1) \cdot \Gamma(\theta)} \cdot \left(\frac{\mu_i}{\theta}\right)^{y_i} \left(\frac{1}{1 + \frac{\mu_i}{\theta}}\right)^{\theta + y_i}$$

$$f_Y(y_i; \theta, \mu_i) = \frac{\Gamma(y_i + \theta)}{\Gamma(y_i + 1) \cdot \Gamma(\theta)} \cdot \left(\frac{\mu_i}{\theta}\right)^{y_i} \left(\frac{\theta}{\theta + \mu_i}\right)^{\theta + y_i}$$

$$f_Y(y_i; \theta, \mu_i) = \frac{\Gamma(y_i + \theta)}{\Gamma(y_i + 1) \cdot \Gamma(\theta)} \cdot \frac{{\mu_i}^{y_i} \theta^{\theta}}{(\theta + \mu_i)^{\theta + y_i}}$$

573

574 **Alternative parametrization of negative binomial regression using a rate model**

575 Alternative parametrization allows STARR-seq data to be modelled as a rate model. In

576 contrast to using input coverage as one of the covariates, we can consider it as

577 "exposure" to output coverage. This "trick" allows us to directly model the basal

bioRxiv preprint doi: https://doi.org/10.1101/694869; this version posted May 5, 2020. The copyright holder for this preprint (which was not certified by peer review) is the author/funder, who has granted bioRxiv a license to display the preprint in perpetuity. It is made available under aCC-BY-NC-ND 4.0 International license.

578 transcription rate (the ratio of RNA to DNA) as a rate response variable. We defined the
579 transcription rate (RNA to DNA ratio) as a new variable, π_i.
580

$$\frac{y_i}{t_i} = \pi_i$$

581
582 If we assume the majority of genomic bins will have the basal transcription rate, we can
583 model the transcription rate at each i-th bin following the traditional negative binomial
584 (NB2) distribution.
585

$$\pi_i \sim NB\left(\frac{\mu_i}{t_i}, \theta\right)$$

586
587 The expected basal transcription, $E(\pi_i)$, becomes the mean incidence rate of y_i per unit
588 of exposure, t_i.
589

$$E\left(\frac{y_i}{t_i}\right) = \frac{\mu_i}{t_i}$$

590
591 By normalizing μ_i by t_i, we are modeling a rate instead of a discrete count using the
592 negative binomial distribution. The regression term for the expected transcription rate
593 can be expressed in terms of a linear combination of explanatory variables, j covariates
594 ($\vec{x}$).
595

bioRxiv preprint doi: https://doi.org/10.1101/694869; this version posted May 5, 2020. The copyright holder for this preprint (which was not certified by peer review) is the author/funder, who has granted bioRxiv a license to display the preprint in perpetuity. It is made available under aCC-BY-NC-ND 4.0 International license.

$$\ln\frac{\mu_i}{t_i} = \beta_1 x_{i1} + \beta_2 x_{i2} + \cdots + \beta_j x_{ij}$$

596

597 Rearranging in terms of the expected value of y, or μ, gives

598

$$\ln\mu_i - \ln t_i = \beta_1 x_{i1} + \beta_2 x_{i2} + \cdots + \beta_j x_{ij}$$

$$\ln\mu_i = \ln t_i + \beta_1 x_{i1} + \beta_2 x_{i2} + \cdots + \beta_j x_{ij}$$

$$\mu_i = \exp\left(\ln t_i + \beta_1 x_{i1} + \beta_2 x_{i2} + \cdots + \beta_j x_{ij}\right)$$

599

600 The natural log of t_i on the RHS ensures μ_i is normalized in the model, acting as an
601 offset variable. In STARRPeaker software, we allow users to optionally choose this
602 alternative rate model (implemented as “mode 2”) instead of the default covariate model
603 described in the main text. This alternate model is useful if constant basal transcription
604 is expected throughout the genome or if covariates are available for directly modelling
605 the basal transcription rate π.

606

607 **BasicSTARRseq**

608 We used BasicSTARRseq R package version 1.10.0 downloaded from Bioconductor
609 (https://bioconductor.org/packages/release/bioc/html/BasicSTARRseq.html). We used
610 default setting as described in the software manual, except for disabling deduplication
611 (minQuantile = 0.9, peakWidth = 500, maxPval = 0.001, deduplicate = FALSE, model =
612 1), to call peaks.

613

614 **MACS2**

bioRxiv preprint doi: https://doi.org/10.1101/694869; this version posted May 5, 2020. The copyright holder for this preprint (which was not certified by peer review) is the author/funder, who has granted bioRxiv a license to display the preprint in perpetuity. It is made available under aCC-BY-NC-ND 4.0 International license.

615 We used MACS2 version 2.1.1 [23] at the recommended default setting, except for
616 allowing duplicates in read (--keep-dup all), since our STARR-seq dataset was
617 multiplexed. We called peaks with an FDR cutoff of 0.01, as recommended by the
618 author of the software.
619

620 **Calculating folding free energy**

621 We used the LinearFold [47] algorithm to estimate the folding energy of each genomic
622 bin iteratively across the whole genome. Specifically, we used the Vienna RNAfold
623 thermodynamic model [48] with parameters from Mathews et al. 2004 [49]. We
624 implemented a parallel processing scheme to leverage multicore processors to expedite
625 the calculation of folding free energy.
626

627 ## Declarations

628 **Availability of data and source codes**

629 We implemented the method described in this article as a Python software package
630 called STARRPeaker. The software package can be downloaded, installed, and readily
631 used to call peaks from any STARR-seq dataset. The STARRPeaker package, as well
632 as source code and documentation, is freely available at:
633 http://github.com/gersteinlab/starrpeaker. All raw data used in the analysis as well as
634 derived resources are available to download from the ENCODE portal
635 (https://www.encodeproject.org/) with accession code ENCSR135NXN for HepG2 and
636 ENCSR858MPS for K562. DNase-seq and ChIP-seq data used for the analysis is also
637 publicly available from the ENCODE portal. The specific accession codes used for the

bioRxiv preprint doi: https://doi.org/10.1101/694869; this version posted May 5, 2020. The copyright holder for this preprint (which was not certified by peer review) is the author/funder, who has granted bioRxiv a license to display the preprint in perpetuity. It is made available under aCC-BY-NC-ND 4.0 International license.

638 analysis are listed in Supplementary Table S3. GC content was downloaded from the
639 UCSC Genome Browser (http://hgdownload.cse.ucsc.edu/gbdb/hg38/bbi/gc5BaseBw/),
640 and the mappability track was created using gem-library software [50] with a k-mer size
641 of 100 bp and the reference human genome build hg38.
642

643 Competing Interests

644 The authors declare that they have no competing interests
645

646 Funding

647 We acknowledge support from the NIH and from the AL Williams Professorship funds.
648

649 Author Contributions

650 D.L., M.S., K.W., and M.G. conceived the project. D.L. and M.G. drafted the manuscript.
651 D.L. developed the STARRPeaker software package. M.S., J.M., M.W., D.F., Y.K., and
652 L.M. performed experimental works. M.W. and Y.K. performed experimental validations.
653 D.L., J.Z., and J.L. performed the downstream analyses. M.G. and K.W. provided
654 funding and supervised the project.
655

656 Acknowledgements

657 We thank Jinrui Xu and Joel Rozowsky for thoughtful discussion about ChIP-seq
658 processing, Michael Rutenberg Schoenberg and Zhen Chen for thoughtful discussion
659 about RNA-folding biology, and all other members of the Gerstein and White
660 laboratories for advice and critical feedback on the manuscript.

bioRxiv preprint doi: https://doi.org/10.1101/694869; this version posted May 5, 2020. The copyright holder for this preprint (which was not certified by peer review) is the author/funder, who has granted bioRxiv a license to display the preprint in perpetuity. It is made available under aCC-BY-NC-ND 4.0 International license.

661

662 ## References

663 1. Muerdter F, Boryń ŁM, Arnold CD. STARR-seq — Principles and applications.
664 Genomics. Academic Press; 2015;106:145–50.
665 2. Yáñez-Cuna JO, Kvon EZ, Stark A. Deciphering the transcriptional cis-regulatory
666 code. Trends Genet. 2013;29:11–22.
667 3. Lettice LA, Heaney SJH, Purdie LA, Li L, de Beer P, Oostra BA, et al. A long-range
668 Shh enhancer regulates expression in the developing limb and fin and is associated
669 with preaxial polydactyly. Hum Mol Genet. 2003;12:1725–35.
670 4. Banerji J, Rusconi S, Schaffner W. Expression of a beta-globin gene is enhanced by
671 remote SV40 DNA sequences. Cell. 1981;27:299–308.
672 5. Sagai T, Hosoya M, Mizushina Y, Tamura M, Shiroishi T. Elimination of a long-range
673 cis-regulatory module causes complete loss of limb-specific Shh expression and
674 truncation of the mouse limb. Development. 2005;132:797–803.
675 6. Melo CA, Drost J, Wijchers PJ, van de Werken H, de Wit E, Vrielink JAFO, et al.
676 eRNAs Are Required for p53-Dependent Enhancer Activity and Gene Transcription. Mol
677 Cell. 2013;49:524–35.
678 7. Sanyal A, Lajoie BR, Jain G, Dekker J. The long-range interaction landscape of gene
679 promoters. Nature. 2012;489:109–13.
680 8. Dao LTM, Galindo-Albarrán AO, Castro-Mondragon JA, Andrieu-Soler C, Medina-
681 Rivera A, Souaid C, et al. Genome-wide characterization of mammalian promoters with
682 distal enhancer functions. Nat Genet. Nature Publishing Group; 2017;49:1073–81.
683 9. Diao Y, Fang R, Li B, Meng Z, Yu J, Qiu Y, et al. A tiling-deletion-based genetic

bioRxiv preprint doi: https://doi.org/10.1101/694869; this version posted May 5, 2020. The copyright holder for this preprint (which was not certified by peer review) is the author/funder, who has granted bioRxiv a license to display the preprint in perpetuity. It is made available under aCC-BY-NC-ND 4.0 International license.

684 screen for cis-regulatory element identification in mammalian cells. Nat Methods.
685 2017;14:629–35.
686 10. Ernst J, Kellis M. ChromHMM: Automating chromatin-state discovery and
687 characterization. Nat Methods. Nature Research; 2012;9:215–6.
688 11. Hoffman MM, Buske OJ, Wang J, Weng Z, Bilmes JA, Noble WS. Unsupervised
689 pattern discovery in human chromatin structure through genomic segmentation. Nat
690 Methods. Nature Publishing Group; 2012;9:473–6.
691 12. Sethi A, Gu M, Gumusgoz E, Chan L, Yan K-K, Rozowsky J, et al. A cross-organism
692 framework for supervised enhancer prediction with epigenetic pattern recognition and
693 targeted validation. bioRxiv. Cold Spring Harbor Laboratory; 2018;385237.
694 13. Patwardhan RP, Hiatt JB, Witten DM, Kim MJ, Smith RP, May D, et al. Massively
695 parallel functional dissection of mammalian enhancers in vivo. Nat Biotechnol. Nature
696 Publishing Group; 2012;30:265–70.
697 14. Melnikov A, Murugan A, Zhang X, Tesileanu T, Wang L, Rogov P, et al. Systematic
698 dissection and optimization of inducible enhancers in human cells using a massively
699 parallel reporter assay. Nat Biotechnol. Nature Publishing Group; 2012;30:271–7.
700 15. Arnold CD, Gerlach D, Stelzer C, Boryń ŁM, Rath M, Stark A. Genome-wide
701 quantitative enhancer activity maps identified by STARR-seq. Science (80-).
702 2013;339:1074–7.
703 16. Liu Y, Yu S, Dhiman VK, Brunetti T, Eckart H, White KP. Functional assessment of
704 human enhancer activities using whole-genome STARR-sequencing. Genome Biol.
705 2017;18:219.
706 17. Klein JC, Agarwal V, Inoue F, Keith A, Martin B, Kircher M, et al. A systematic

bioRxiv preprint doi: https://doi.org/10.1101/694869; this version posted May 5, 2020. The copyright holder for this preprint (which was not certified by peer review) is the author/funder, who has granted bioRxiv a license to display the preprint in perpetuity. It is made available under aCC-BY-NC-ND 4.0 International license.

707 evaluation of the design, orientation, and sequence context dependencies of massively
708 parallel reporter assays. bioRxiv. Cold Spring Harbor Laboratory; 2019;576405.
709 18. Johnson GD, Barrera A, McDowell IC, D'Ippolito AM, Majoros WH, Vockley CM, et
710 al. Human genome-wide measurement of drug-responsive regulatory activity. Nat
711 Commun. 2018;9:5317.
712 19. Rathert P, Roth M, Neumann T, Muerdter F, Roe J-S, Muhar M, et al.
713 Transcriptional plasticity promotes primary and acquired resistance to BET inhibition.
714 Nature. 2015;525:543–7.
715 20. Koohy H, Down TA, Spivakov M, Hubbard T. A comparison of peak callers used for
716 DNase-Seq data. Helmer-Citterich M, editor. PLoS One. 2014;9:e96303.
717 21. Uren PJ, Bahrami-Samani E, Burns SC, Qiao M, Karginov F V, Hodges E, et al. Site
718 identification in high-throughput RNA-protein interaction data. Bioinformatics. Oxford
719 University Press; 2012;28:3013–20.
720 22. Strbenac D, Armstrong NJ, Yang JYH. Detection and classification of peaks in 5'
721 cap RNA sequencing data. BMC Genomics. BioMed Central; 2013;14 Suppl 5:S9.
722 23. Zhang Y, Liu T, Meyer CA, Eeckhoute J, Johnson DS, Bernstein BE, et al. Model-
723 based Analysis of ChIP-Seq (MACS). Genome Biol. BioMed Central; 2008;9:R137.
724 24. Kharchenko P V, Tolstorukov MY, Park PJ. Design and analysis of ChIP-seq
725 experiments for DNA-binding proteins. Nat Biotechnol. Nature Publishing Group;
726 2008;26:1351–9.
727 25. Li H, Handsaker B, Wysoker A, Fennell T, Ruan J, Homer N, et al. The Sequence
728 Alignment/Map format and SAMtools. Bioinformatics. 2009;25:2078–9.
729 26. Poptsova MS, Il'icheva IA, Nechipurenko DY, Panchenko LA, Khodikov M V,

bioRxiv preprint doi: https://doi.org/10.1101/694869; this version posted May 5, 2020. The copyright holder for this preprint (which was not certified by peer review) is the author/funder, who has granted bioRxiv a license to display the preprint in perpetuity. It is made available under aCC-BY-NC-ND 4.0 International license.

730 Oparina NY, et al. Non-random DNA fragmentation in next-generation sequencing. Sci
731 Rep. 2014;4:4532.
732 27. Lazarovici A, Zhou T, Shafer A, Dantas Machado AC, Riley TR, Sandstrom R, et al.
733 Probing DNA shape and methylation state on a genomic scale with DNase I. Proc Natl
734 Acad Sci U S A. 2013;110:6376–81.
735 28. Lai D, Proctor JR, Meyer IM. On the importance of cotranscriptional RNA structure
736 formation. RNA. 2013;19:1461–73.
737 29. Ringnér M, Krogh M. Folding free energies of 5’-UTRs impact post-transcriptional
738 regulation on a genomic scale in yeast. PLoS Comput Biol. 2005;1:e72.
739 30. Rabani M, Levin JZ, Fan L, Adiconis X, Raychowdhury R, Garber M, et al. Metabolic
740 labeling of RNA uncovers principles of RNA production and degradation dynamics in
741 mammalian cells. Nat Biotechnol. 2011;29:436–42.
742 31. Yang E, van Nimwegen E, Zavolan M, Rajewsky N, Schroeder M, Magnasco M, et
743 al. Decay rates of human mRNAs: Correlation with functional characteristics and
744 sequence attributes. Genome Res. 2003;13:1863–72.
745 32. Tani H, Mizutani R, Salam KA, Tano K, Ijiri K, Wakamatsu A, et al. Genome-wide
746 determination of RNA stability reveals hundreds of short-lived noncoding transcripts in
747 mammals. Genome Res. 2012;22:947–56.
748 33. Papoulis A, Athanasios. Probability, random variables and stochastic processes.
749 New York McGraw-Hill, 1984, 2nd ed. 1984;
750 34. Pang B, Snyder MP. Systematic identification of silencers in human cells. Nat Genet.
751 Nature Publishing Group; 2020;52:1–10.
752 35. Hilbe JM. Negative Binomial Regression [Internet]. Cambridge: Cambridge

bioRxiv preprint doi: https://doi.org/10.1101/694869; this version posted May 5, 2020. The copyright holder for this preprint (which was not certified by peer review) is the author/funder, who has granted bioRxiv a license to display the preprint in perpetuity. It is made available under aCC-BY-NC-ND 4.0 International license.

753 University Press; 2011.
754 36. Cameron ACA, Trivedi PK. Regression Analysis of Count Data [Internet].
755 Cambridge: Cambridge University Press; 2013.
756 37. Hilbe JM. Modeling Count Data [Internet]. Cambridge: Cambridge University Press;
757 2014.
758 38. Benjamini Y, Hochberg Y. Controlling the False Discovery Rate: A Practical and
759 Powerful Approach to Multiple Testing. J R Stat Soc Ser B. John Wiley & Sons, Ltd
760 (10.1111); 1995;57:289–300.
761 39. Muerdter F, Boryń ŁM, Woodfin AR, Neumayr C, Rath M, Zabidi MA, et al.
762 Resolving systematic errors in widely used enhancer activity assays in human cells. Nat
763 Methods. Nature Publishing Group; 2018;15:141–9.
764 40. Pennacchio LA, Bickmore W, Dean A, Nobrega MA, Bejerano G. Enhancers: five
765 essential questions. Nat Rev Genet. NIH Public Access; 2013;14:288–95.
766 41. Kawaji H, Kasukawa T, Forrest A, Carninci P. The FANTOM 5 collection, a data
767 series underpinning mammalian transcriptome atlases in diverse cell types. Sci Data.
768 2017;2016–8.
769 42. Inoue F, Kircher M, Martin B, Cooper GM, Witten DM, McManus MT, et al. A
770 systematic comparison reveals substantial differences in chromosomal versus episomal
771 encoding of enhancer activity. Genome Res. 2017;27:38–52.
772 43. Wang X, He L, Goggin SM, Saadat A, Wang L, Sinnott-Armstrong N, et al. High-
773 resolution genome-wide functional dissection of transcriptional regulatory regions and
774 nucleotides in human. Nat Commun. Nature Publishing Group; 2018;9:1–15.
775 44. Dixit A, Parnas O, Li B, Chen J, Fulco CP, Jerby-Arnon L, et al. Perturb-Seq:

bioRxiv preprint doi: https://doi.org/10.1101/694869; this version posted May 5, 2020. The copyright holder for this preprint (which was not certified by peer review) is the author/funder, who has granted bioRxiv a license to display the preprint in perpetuity. It is made available under aCC-BY-NC-ND 4.0 International license.

776 Dissecting Molecular Circuits with Scalable Single-Cell RNA Profiling of Pooled Genetic
777 Screens. Cell. Cell Press; 2016;167:1853-1866.e17.
778 45. Xie S, Duan J, Li B, Zhou P, Hon GC. Multiplexed Engineering and Analysis of
779 Combinatorial Enhancer Activity in Single Cells. Mol Cell. Cell Press; 2017;66:285-
780 299.e5.
781 46. Gasperini M, Hill AJ, McFaline-Figueroa JL, Martin B, Kim S, Zhang MD, et al. A
782 Genome-wide Framework for Mapping Gene Regulation via Cellular Genetic Screens.
783 Cell. Cell Press; 2019;176:377-390.e19.
784 47. Huang L, Zhang H, Deng D, Zhao K, Liu K, Hendrix DA, et al. LinearFold: linear-
785 time approximate RNA folding by 5'-to-3' dynamic programming and beam search.
786 Bioinformatics. Narnia; 2019;35:i295–304.
787 48. Lorenz R, Bernhart SH, Höner zu Siederdissen C, Tafer H, Flamm C, Stadler PF, et
788 al. ViennaRNA Package 2.0. Algorithms Mol Biol. BioMed Central; 2011;6:26.
789 49. Mathews DH, Disney MD, Childs JL, Schroeder SJ, Zuker M, Turner DH.
790 Incorporating chemical modification constraints into a dynamic programming algorithm
791 for prediction of RNA secondary structure. Proc Natl Acad Sci U S A. National Academy
792 of Sciences; 2004;101:7287–92.
793 50. Derrien T, Estellé J, Marco Sola S, Knowles DG, Raineri E, Guigó R, et al. Fast
794 Computation and Applications of Genome Mappability. Ouzounis CA, editor. PLoS One.
795 2012;7:e30377.
796

797 ## Supplementary Tables

798 **Table S1** contains significant peaks called by STARRPeaker.

bioRxiv preprint doi: https://doi.org/10.1101/694869; this version posted May 5, 2020. The copyright holder for this preprint (which was not certified by peer review) is the author/funder, who has granted bioRxiv a license to display the preprint in perpetuity. It is made available under aCC-BY-NC-ND 4.0 International license.

799 **Table S2** contains overlap of various peak callers (STARRPeaker, BasicSTARRseq,
800 and MACS2) to published enhancers identified using other types of enhancer assays.
801 **Table S3** contains a list of data sources and accession numbers used for the analysis.
802 **Table S4** compares peaks identified by various peak callers (STARRPeaker,
803 BasicSTARRseq, and MACS2).
804

805 Supplementary Figures

806 **Supplementary Figure 1** Comparison of STARR-seq output coverage calculated using
807 the center of the fragment to using the start position of the sequencing read. **(A)**
808 Distribution of shift in final peak locations resulting from using two alternative coverage
809 counting schemes in HepG2. Comparison of **(B)** overall fold enrichment level, **(C)** p-
810 value, and **(D)** size of resulting peaks.
811
812 **Supplementary Figure 2** Contribution of covariates and model selection. **(A)** Q-Q plots
813 of various models with different sets of covariates showing the goodness of fit. **(B)** Both
814 AIC and BIC measure relative qualities of statistical models considering the trade-off
815 between the goodness of fit and the simplicity of the model. AIC: Akaike information
816 criterion; BIC: Bayesian information criterion.
817
818 **Supplementary Figure 3** Correlation between replicates for **(A)** HepG2 or **(B)** K562 cell
819 lines.
820

bioRxiv preprint doi: https://doi.org/10.1101/694869; this version posted May 5, 2020. The copyright holder for this preprint (which was not certified by peer review) is the author/funder, who has granted bioRxiv a license to display the preprint in perpetuity. It is made available under aCC-BY-NC-ND 4.0 International license.

821 **Supplementary Figure 4** Comparison of peaks called from subsamples of the original
822 STARR-seq library, highlighting the robustness of STARRPeaker.
823
824 **Supplementary Figure 5** Orientation biases analysis for **(A-B)** HepG2 or **(C-D)** K562
825 cell lines. The ratio between forward and reverse stranded fragments was tested for
826 statistical significance using a binomial test. Orange dots represent peaks with
827 significant strand bias (FDR q-value < 0.01).
828
829 **Supplementary Figure 6** Comparison of peaks identified by various methods using a
830 simulated STARR-seq dataset containing four spike-in control regions.
831
832 **Supplementary Figure 7** Enrichment of epigenetic signals around peaks in K562. All
833 peaks were centered at the summit, uniformly thresholded using P-value < 0.001, and
834 10,000 peaks were randomly selected. Aggregated read depth at 2,000 bp upstream
835 and downstream were plotted for **(A)** DNase I hypersensitive sites (DHS), **(B)** H3K27ac,
836 **(C)** H3K4me1, and **(D)** aggregated TF ChIP-seq profile. For DNase-seq, enrichment
837 indicates unique read depth. For histone ChIP-seq, enrichment indicates fold change
838 over control. For TF ChIP-seq aggregate, enrichment indicates the number of TFs
839 binding.
840
841 **Supplementary Figure 8 (A-C)** Genome browser session comparing STARRPeaker to
842 other peak-calling methods at validated enhancers from CRISPRi.
843

bioRxiv preprint doi: https://doi.org/10.1101/694869; this version posted May 5, 2020. The copyright holder for this preprint (which was not certified by peer review) is the author/funder, who has granted bioRxiv a license to display the preprint in perpetuity. It is made available under aCC-BY-NC-ND 4.0 International license.

Supplementary Figure 9 Application of STARRPeaker on an external HeLa-S3 dataset. **(A)** Comparison of chromatin accessibility (DNase-seq) for STARRPeaker peaks between untreated and inhibitor-treated samples. **(B)** Comparison of STARRPeaker peaks to published results. STARRPeaker found 6,540 additional peaks that are enriched with chromatin accessibility signals from a HeLa-S3 sample.

Supplementary Figure 10 Venn diagram for four-way comparison of peaks identified by various methods using a published dataset from Rathert et al. 2015.

Figure legends

Figure 1 Comparison of STARR-seq output coverage calculated using the center of the fragment to using the start position of the sequencing read. **(A)** Distribution of the shift in final peak locations resulting from using two alternative coverage counting schemes in HepG2. Comparison of **(B)** overall fold enrichment level, **(C)** p-value, and **(D)** size of resulting peaks. **(E)** Example highlighting the difference between fragment-based and read-based coverage counting schemes and their resulting peak calls from HepG2 STARR-seq data. Asterisks represents statistical significance using the Mann-Whitney-Wilcoxon test two-sided with Bonferroni correction; (*) P <= 0.05, (**) P <= 0.01, (***) P <= 0.001, (****) P <= 0.0001.

Figure 2 Confounding factors in the STARR-seq assay. STARR-seq output and input coverages are significantly correlated with **(A)** input coverage, **(B)** GC content, **(C)**

bioRxiv preprint doi: https://doi.org/10.1101/694869; this version posted May 5, 2020. The copyright holder for this preprint (which was not certified by peer review) is the author/funder, who has granted bioRxiv a license to display the preprint in perpetuity. It is made available under aCC-BY-NC-ND 4.0 International license.

866 mappability, and **(D)** RNA structure folding. PCC: Pearson Correlation Coefficient. Plots
867 were from a sampling of 5,000 random genomic bins.
868
869 **Figure 3** STARR-seq output coverage is fitted against simulated coverage using three
870 distribution models; negative binomial, binomial, and Poisson. **(A)** Density histogram of
871 simulated distribution against STARR-seq output coverage. **(B)** Q-Q plot of simulated
872 distribution against STARR-seq output coverage. The red solid line represents where
873 the observed count equals the expected count.
874
875 **Figure 4** Overview of STARRPeaker peak-calling scheme. **(A)** In contrast to using read
876 depth (grey), fragment depth (red) offers more precise and sharper STARR-seq output
877 coverage. Fragment inserts are directly inferred from properly paired-reads. **(B)**
878 Workflow of STARRPeaker describing how coverage is calculated for each genomic bin
879 and modelled using a negative binomial regression model. The analysis pipeline can
880 largely be divided into four steps: (1) Binning the genome; (2) calculating coverage and
881 computing covariate matrix; (3) fitting the STARR-seq data to the NB regression model;
882 and (4) peak calling, multiple hypothesis testing correction, and adjustment of the center
883 of peaks.
884
885 **Figure 5** Enrichment of epigenetic signals around peaks in HepG2. All peaks were
886 centered at the summit, uniformly thresholded using P-value < 0.001, and 10,000 peaks
887 were randomly selected. Aggregated read depth at 2,000 bp upstream and downstream
888 were plotted for **(A)** DNase I hypersensitive sites (DHS), **(B)** H3K27ac, **(C)** H3K4me1,

bioRxiv preprint doi: https://doi.org/10.1101/694869; this version posted May 5, 2020. The copyright holder for this preprint (which was not certified by peer review) is the author/funder, who has granted bioRxiv a license to display the preprint in perpetuity. It is made available under aCC-BY-NC-ND 4.0 International license.

889 and **(D)** aggregated TF ChIP-seq profile. For DNase-seq, enrichment indicates unique
890 read depth. For histone ChIP-seq, enrichment indicates fold change over control. For
891 TF ChIP-seq aggregate, enrichment indicates the number of TFs binding.
892
893 **Figure 6** Comparison of peaks using an external dataset for **(A)** HepG2 or **(B)** K562 cell
894 lines. Peaks identified from STARRPeaker as well as BasicSTARRseq and MACS2
895 were compared against a published dataset. For a fair comparison, all peaks were
896 centered at the summit, uniformly thresholded using P-value < 0.001, and 20,000 peaks
897 were randomly drawn from peaks identified by each peak caller using the recommended
898 settings. The fraction of overlap was computed for each replicate. We considered it an
899 overlap when at least 50% of peaks intersected each other.

bioRxiv preprint doi: https://doi.org/10.1101/694869; this version posted May 5, 2020. The copyright holder for this preprint (which was not certified by peer review) is the author/funder, who has granted bioRxiv a license to display the preprint in perpetuity. It is made available under aCC-BY-NC-ND 4.0 International license.

Figure 1

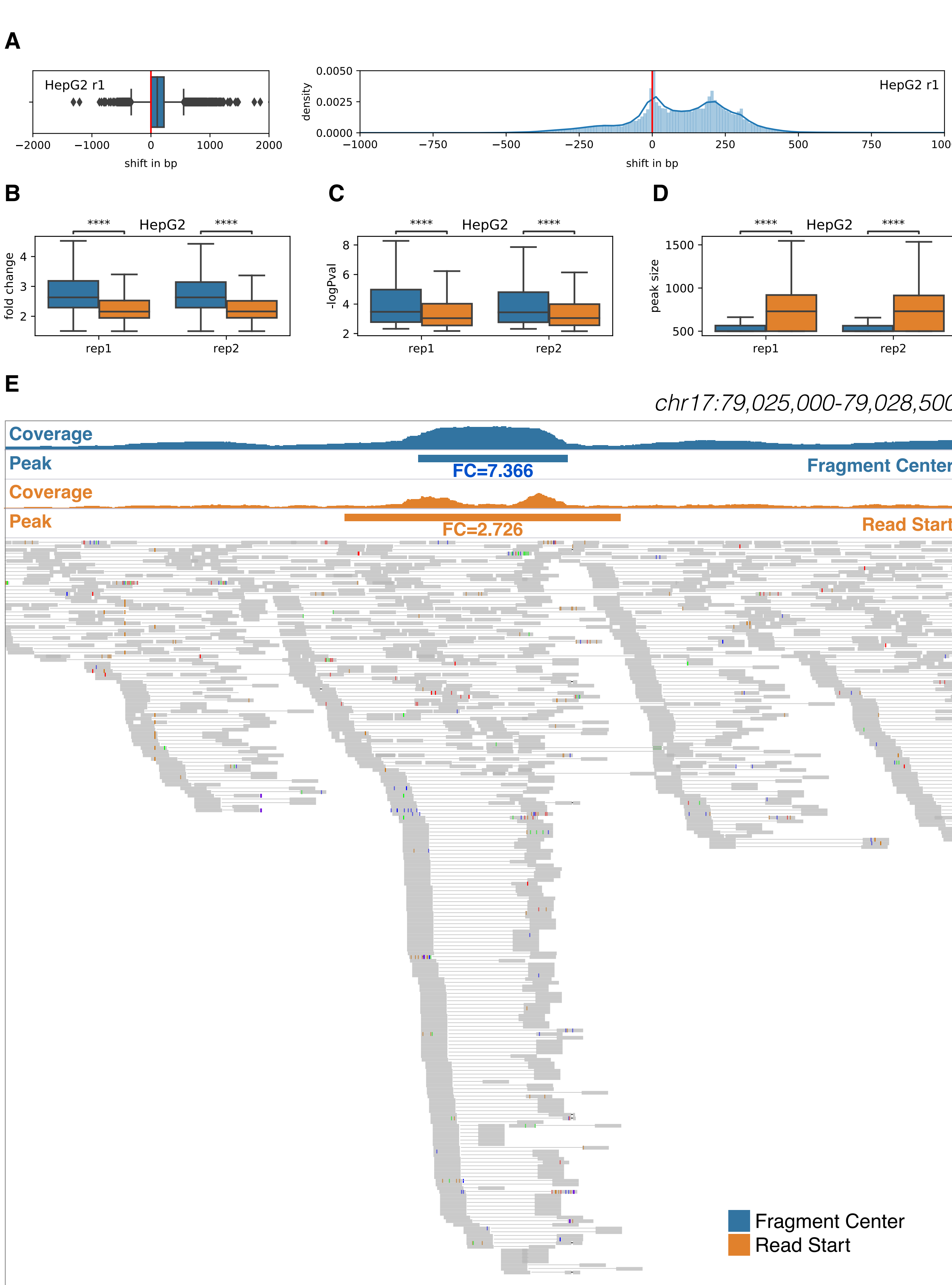

bioRxiv preprint doi: https://doi.org/10.1101/694869; this version posted May 5, 2020. The copyright holder for this preprint (which was not certified by peer review) is the author/funder, who has granted bioRxiv a license to display the preprint in perpetuity. It is made available under aCC-BY-NC-ND 4.0 International license.

Figure 2

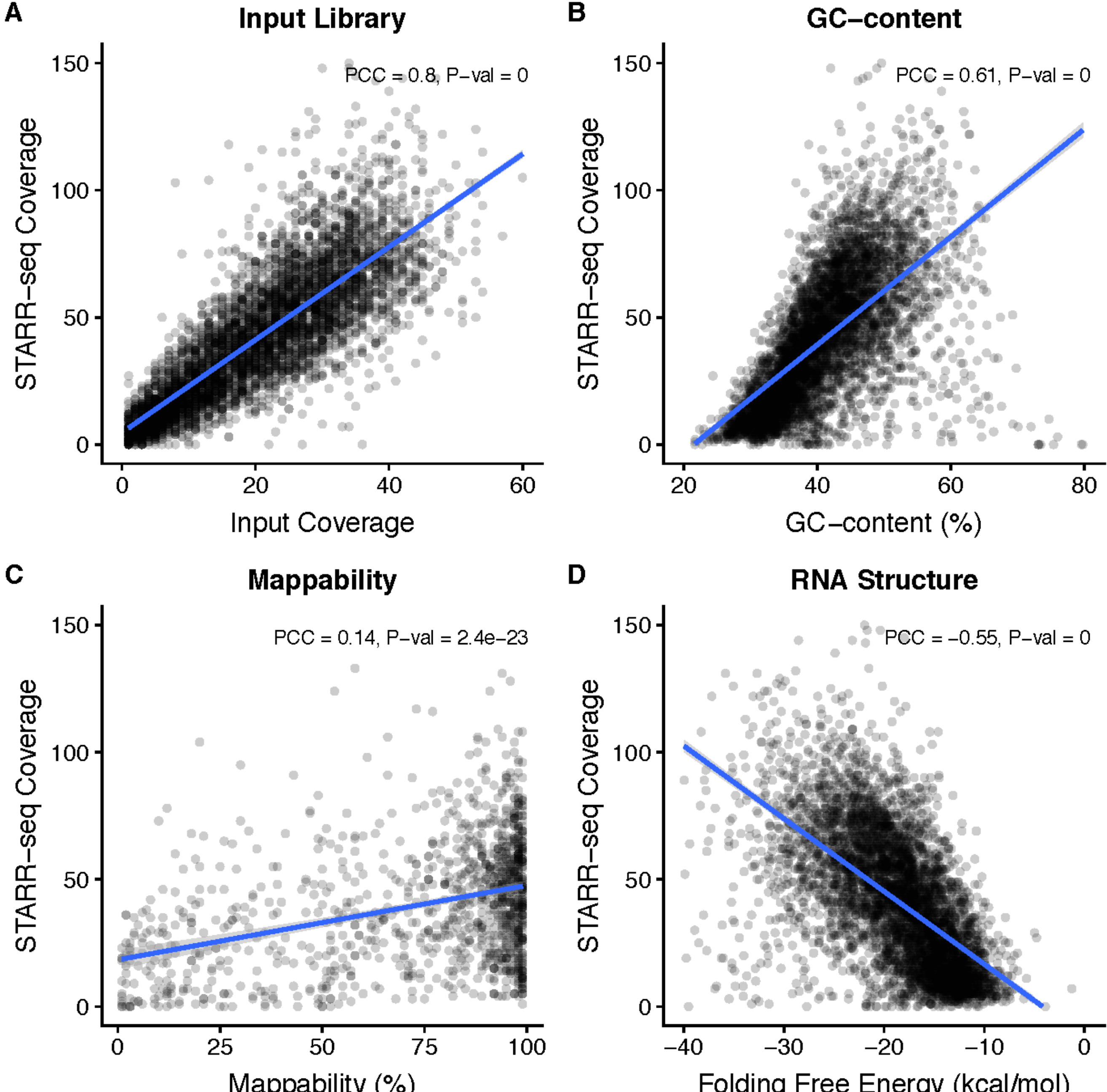

bioRxiv preprint doi: https://doi.org/10.1101/694869; this version posted May 5, 2020. The copyright holder for this preprint (which was not certified by peer review) is the author/funder, who has granted bioRxiv a license to display the preprint in perpetuity. It is made available under aCC-BY-NC-ND 4.0 International license.

Figure 3

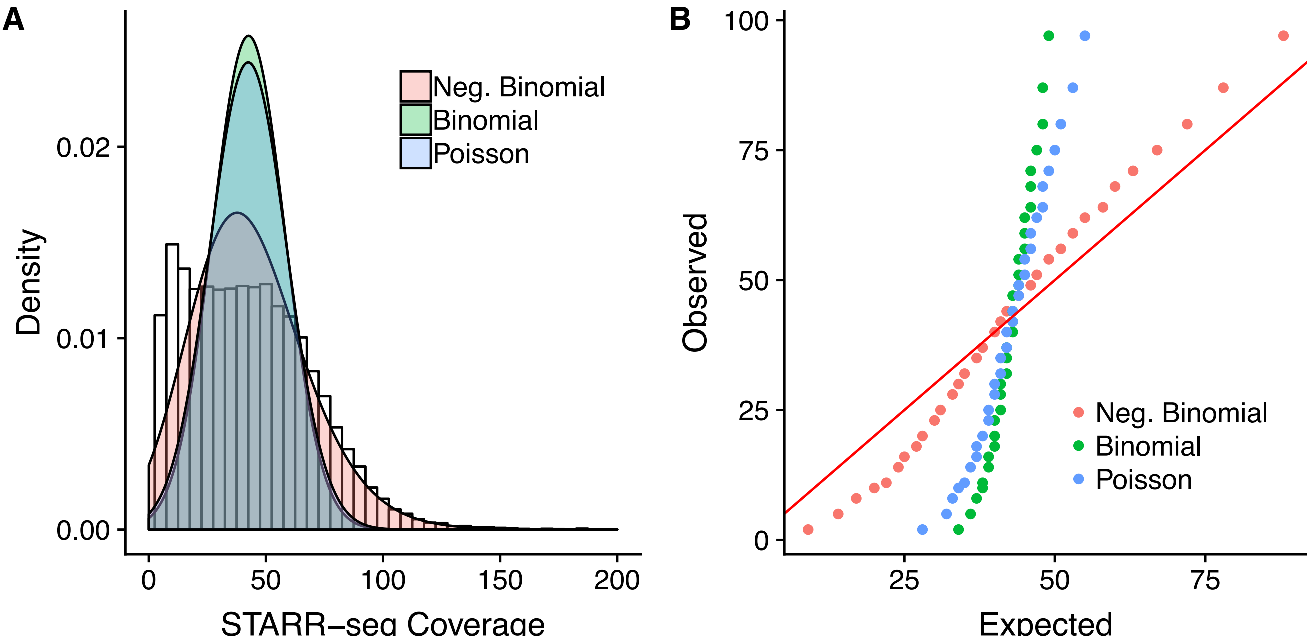

bioRxiv preprint doi: https://doi.org/10.1101/694869; this version posted May 5, 2020. The copyright holder for this preprint (which was not certified by peer review) is the author/funder, who has granted bioRxiv a license to display the preprint in perpetuity. It is made available under aCC-BY-NC-ND 4.0 International license.

Figure 4

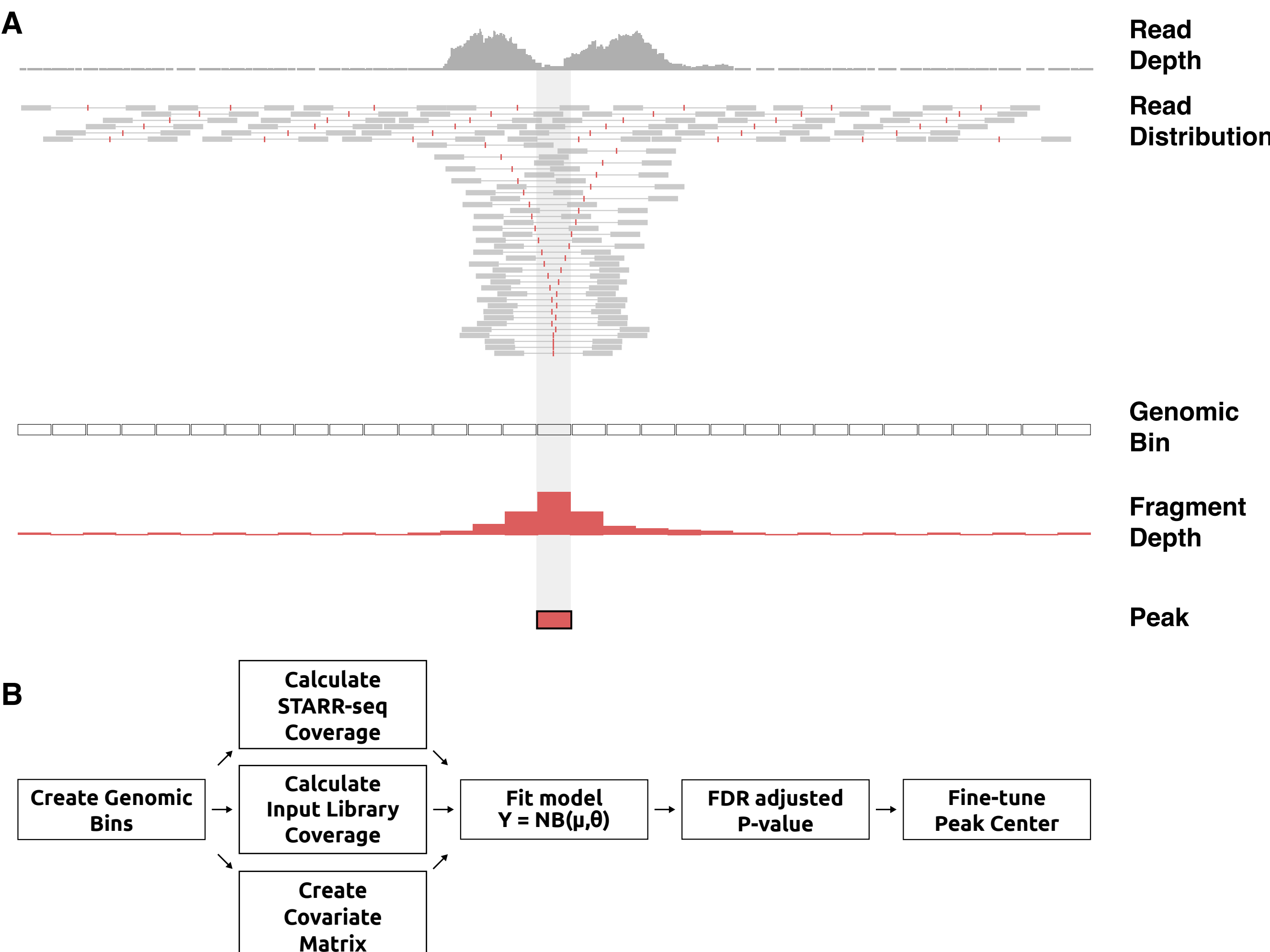

bioRxiv preprint doi: https://doi.org/10.1101/694869; this version posted May 5, 2020. The copyright holder for this preprint (which was not certified by peer review) is the author/funder, who has granted bioRxiv a license to display the preprint in perpetuity. It is made available under aCC-BY-NC-ND 4.0 International license.

Figure 5

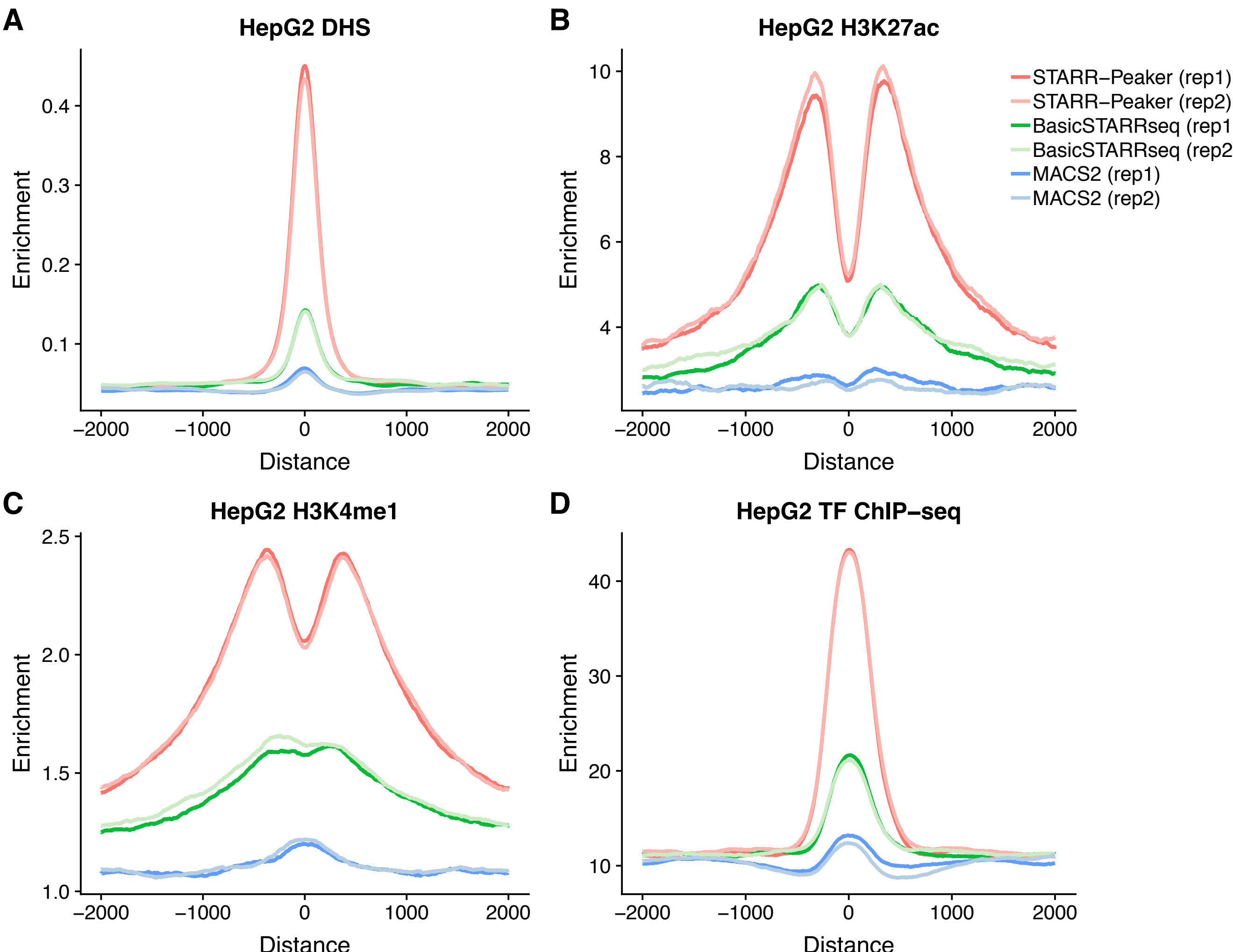

bioRxiv preprint doi: https://doi.org/10.1101/694869; this version posted May 5, 2020. The copyright holder for this preprint (which was not certified by peer review) is the author/funder, who has granted bioRxiv a license to display the preprint in perpetuity. It is made available under aCC-BY-NC-ND 4.0 International license.

Figure 6

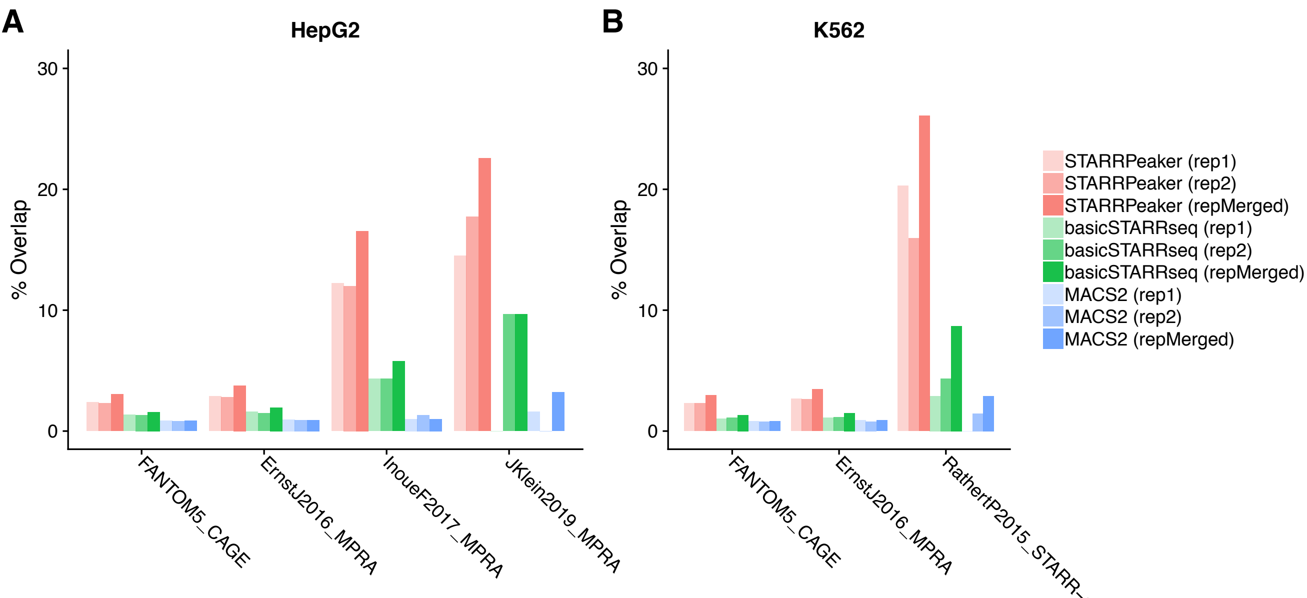

bioRxiv preprint doi: https://doi.org/10.1101/694869; this version posted May 5, 2020. The copyright holder for this preprint (which was not certified by peer review) is the author/funder, who has granted bioRxiv a license to display the preprint in perpetuity. It is made available under aCC-BY-NC-ND 4.0 International license.

Supplementary Figure 1

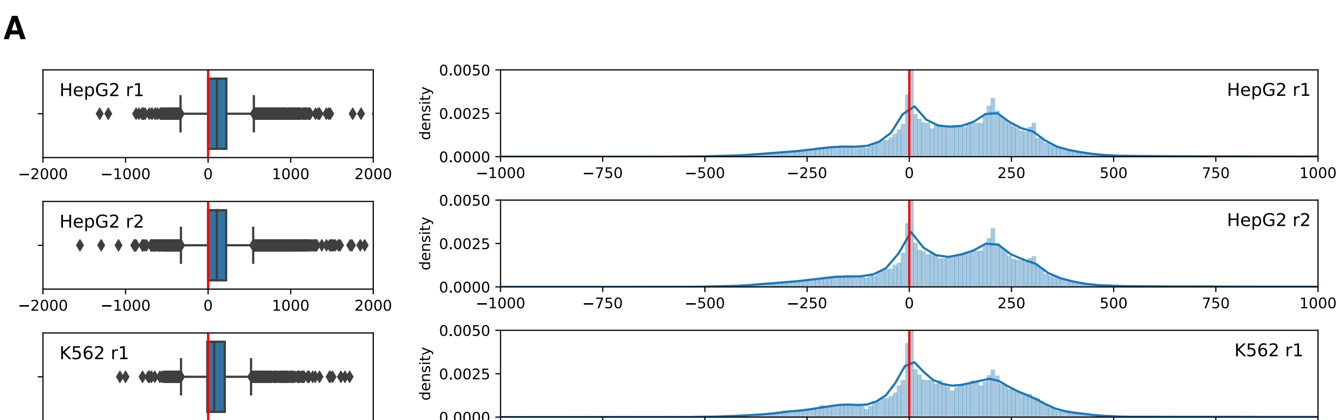

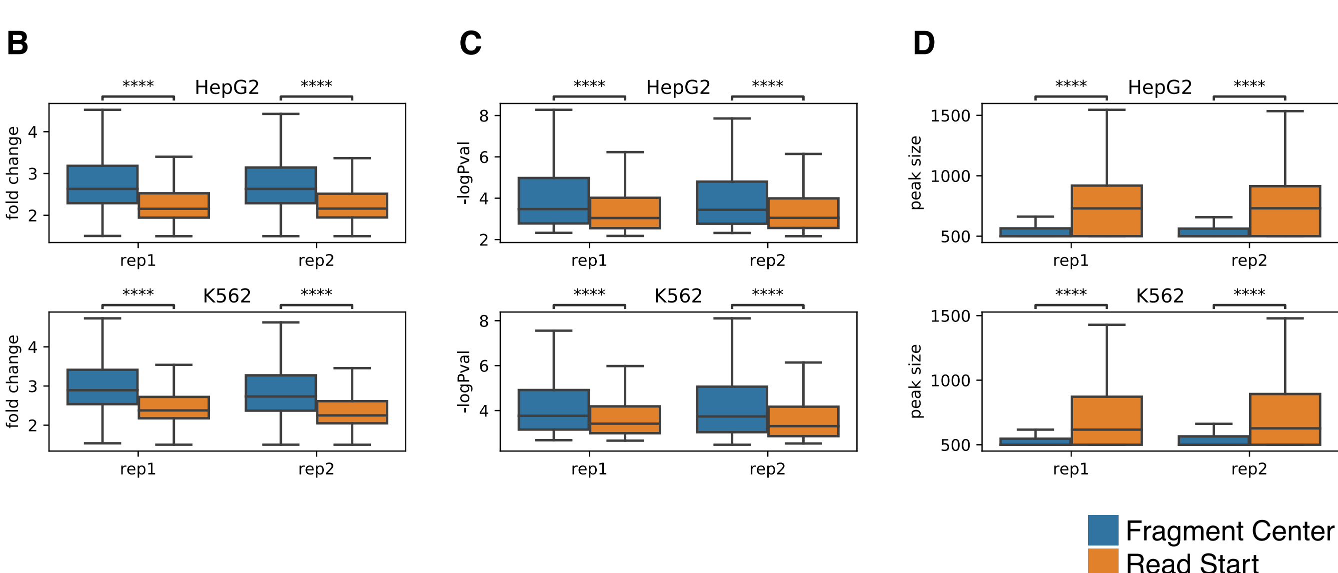

bioRxiv preprint doi: https://doi.org/10.1101/694869; this version posted May 5, 2020. The copyright holder for this preprint (which was not certified by peer review) is the author/funder, who has granted bioRxiv a license to display the preprint in perpetuity. It is made available under aCC-BY-NC-ND 4.0 International license.

Supplementary Figure 2

A

DNA only, AIC=8.532e+05, BIC=-1.055e+06

DNA+GC, AIC=8.491e+05, BIC=-1.059e+06

DNA+GC+MAP, AIC=8.476e+05, BIC=-1.061e+06

DNA+GC+MAP+FOLD, AIC=8.473e+05, BIC=-1.061e+06

Sample Quantiles

Theoretical Quantiles

B

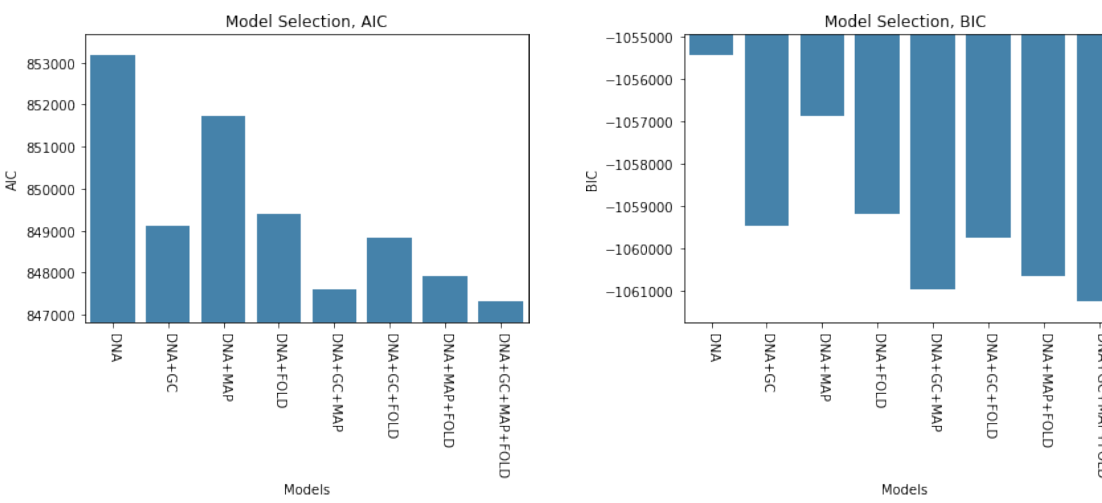

bioRxiv preprint doi: https://doi.org/10.1101/694869; this version posted May 5, 2020. The copyright holder for this preprint (which was not certified by peer review) is the author/funder, who has granted bioRxiv a license to display the preprint in perpetuity. It is made available under aCC-BY-NC-ND 4.0 International license.

Supplementary Figure 3

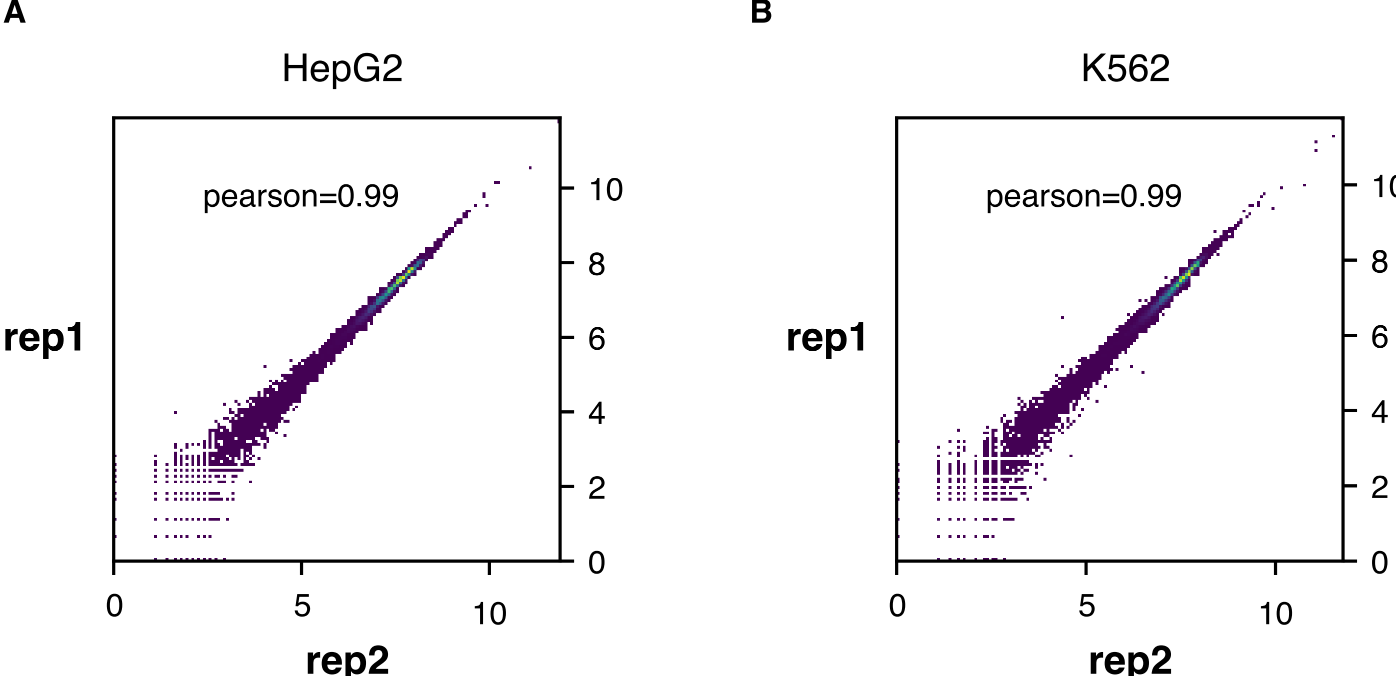

bioRxiv preprint doi: https://doi.org/10.1101/694869; this version posted May 5, 2020. The copyright holder for this preprint (which was not certified by peer review) is the author/funder, who has granted bioRxiv a license to display the preprint in perpetuity. It is made available under aCC-BY-NC-ND 4.0 International license.

Supplementary Figure 4

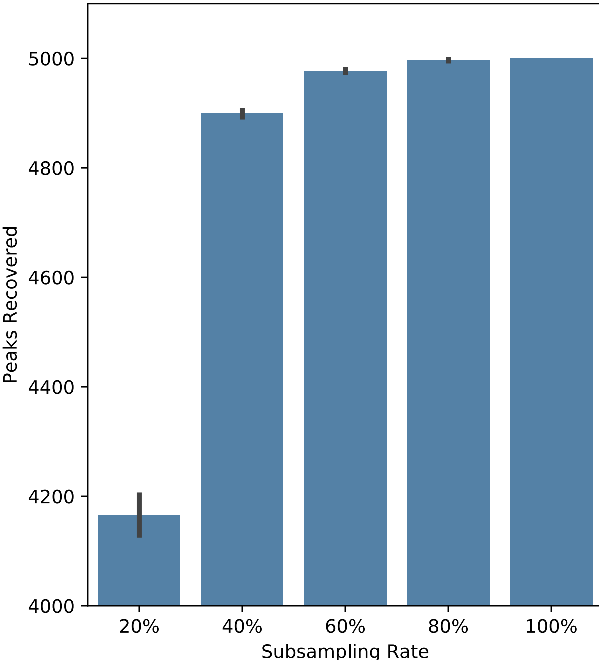

bioRxiv preprint doi: https://doi.org/10.1101/694869; this version posted May 5, 2020. The copyright holder for this preprint (which was not certified by peer review) is the author/funder, who has granted bioRxiv a license to display the preprint in perpetuity. It is made available under aCC-BY-NC-ND 4.0 International license.

Supplementary Figure 5

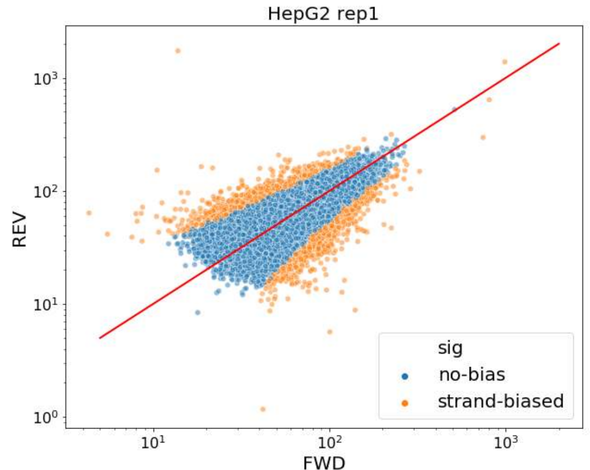

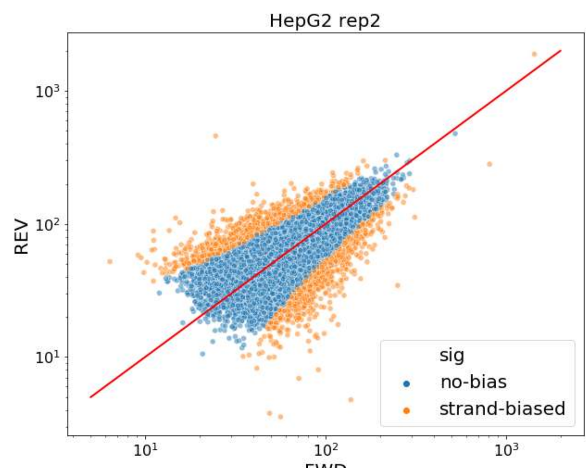

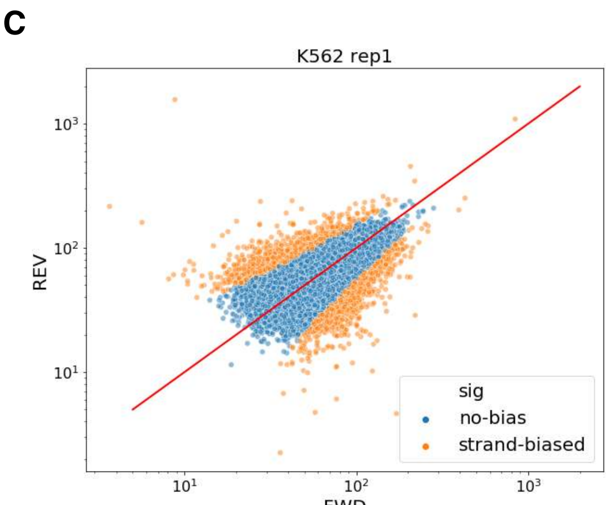

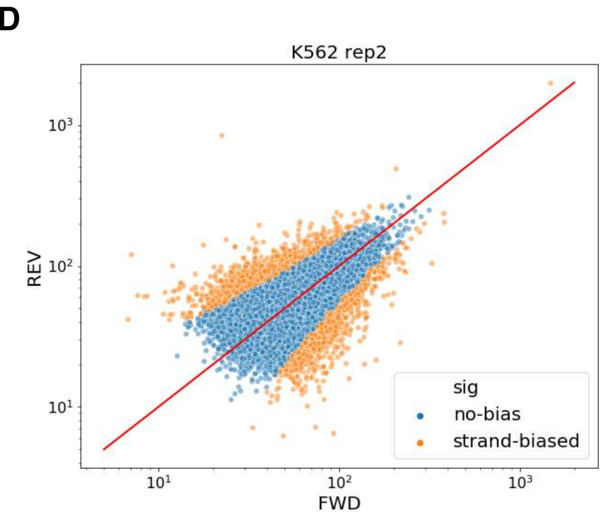

bioRxiv preprint doi: https://doi.org/10.1101/694869; this version posted May 5, 2020. The copyright holder for this preprint (which was not certified by peer review) is the author/funder, who has granted bioRxiv a license to display the preprint in perpetuity. It is made available under aCC-BY-NC-ND 4.0 International license.

Supplementary Figure 6

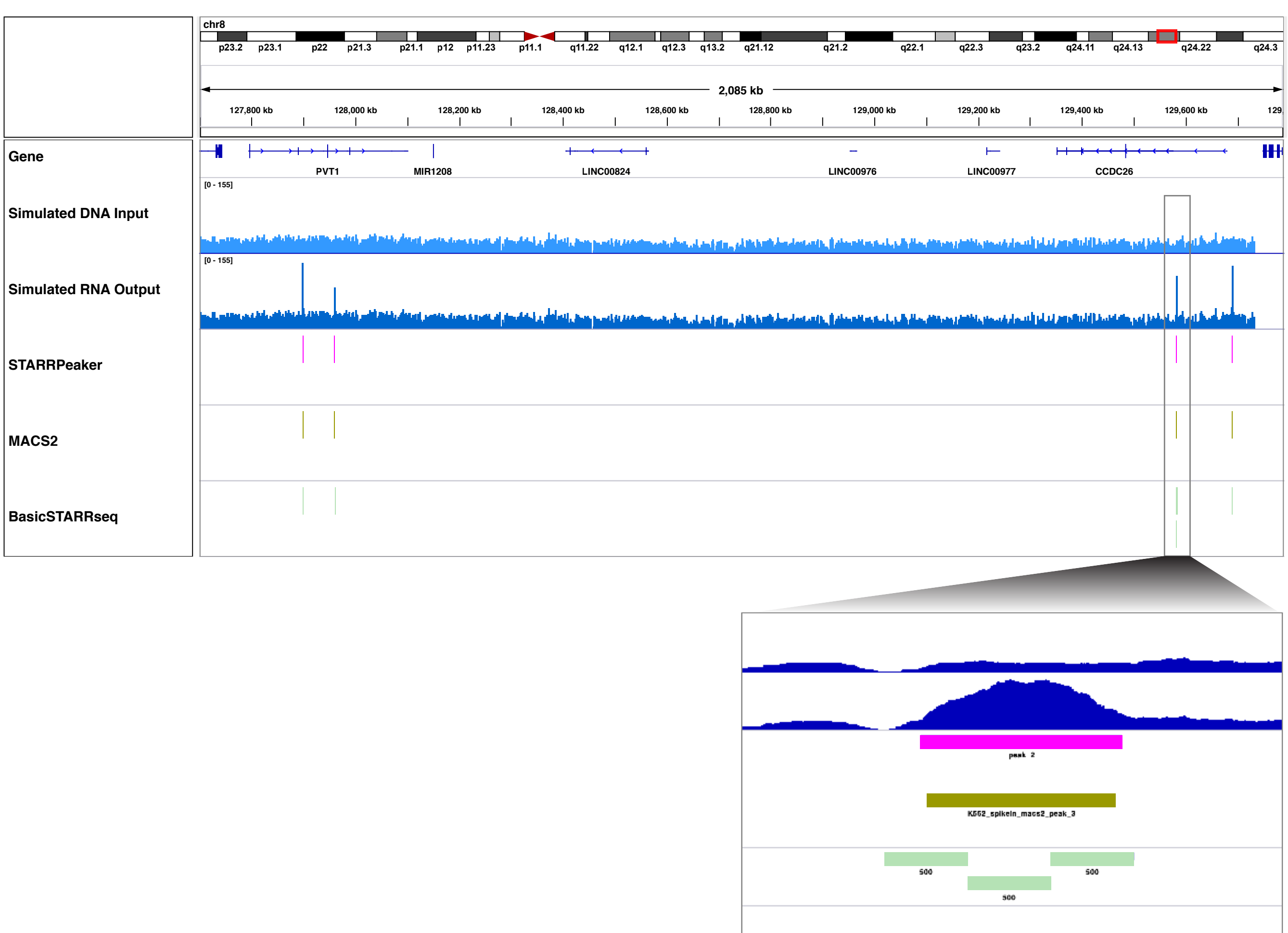

bioRxiv preprint doi: https://doi.org/10.1101/694869; this version posted May 5, 2020. The copyright holder for this preprint (which was not certified by peer review) is the author/funder, who has granted bioRxiv a license to display the preprint in perpetuity. It is made available under aCC-BY-NC-ND 4.0 International license.

Supplementary Figure 7

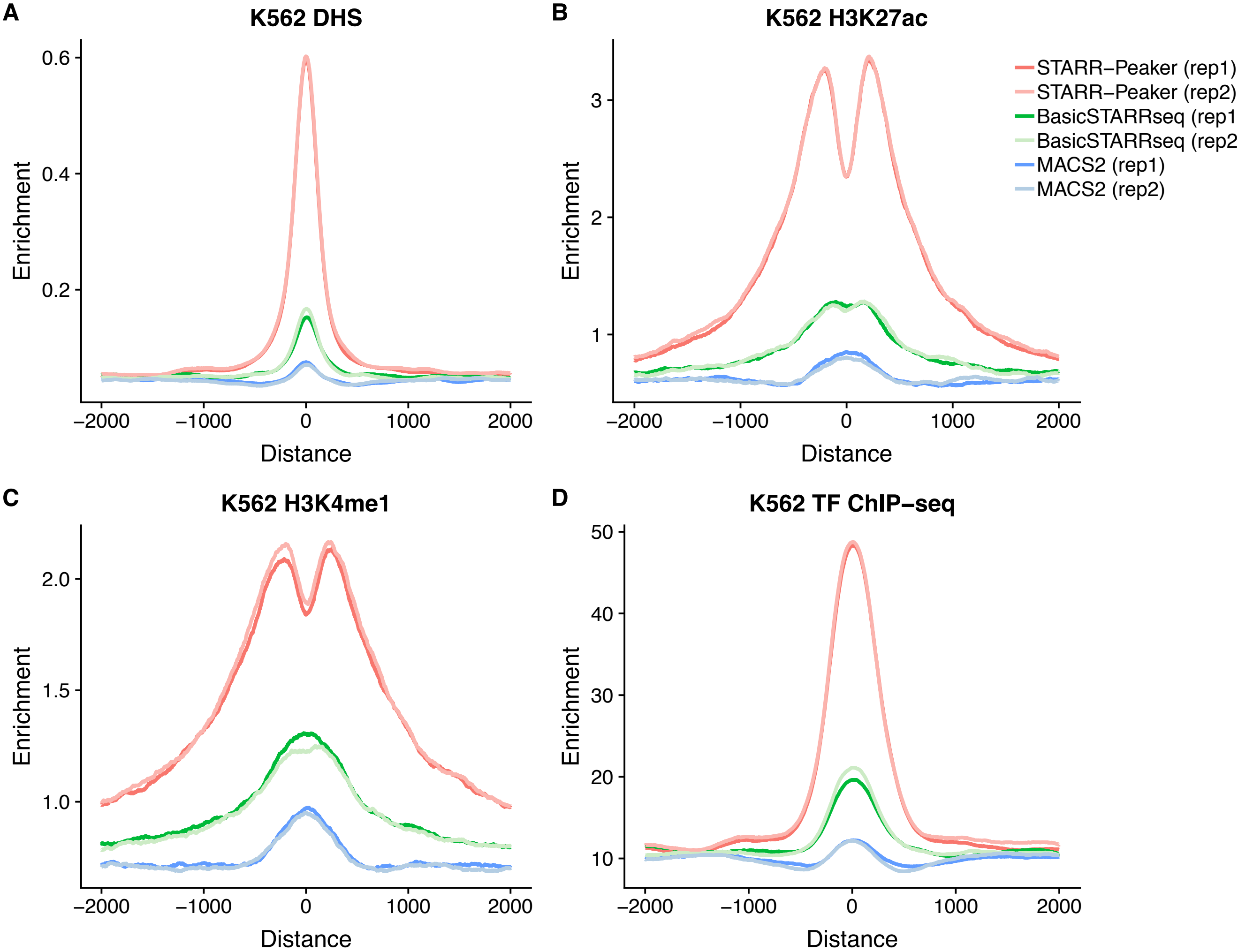

bioRxiv preprint doi: https://doi.org/10.1101/694869; this version posted May 5, 2020. The copyright holder for this preprint (which was not certified by peer review) is the author/funder, who has granted bioRxiv a license to display the preprint in perpetuity. It is made available under aCC-BY-NC-ND 4.0 International license.

Supplementary Figure 8

A GATA1 locus chrX:48774179-48806695

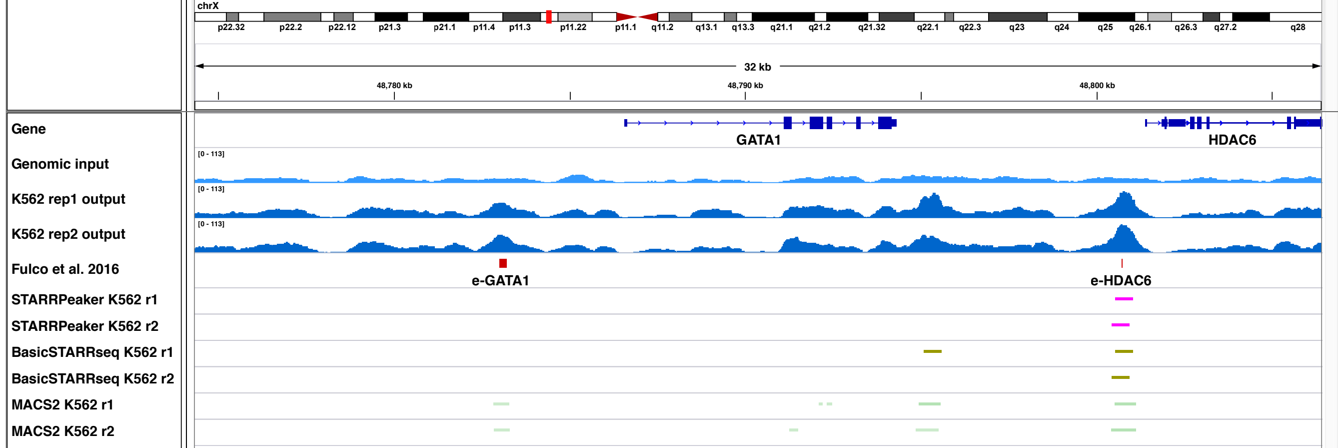

B MYC locus chr8:127830000-128090000

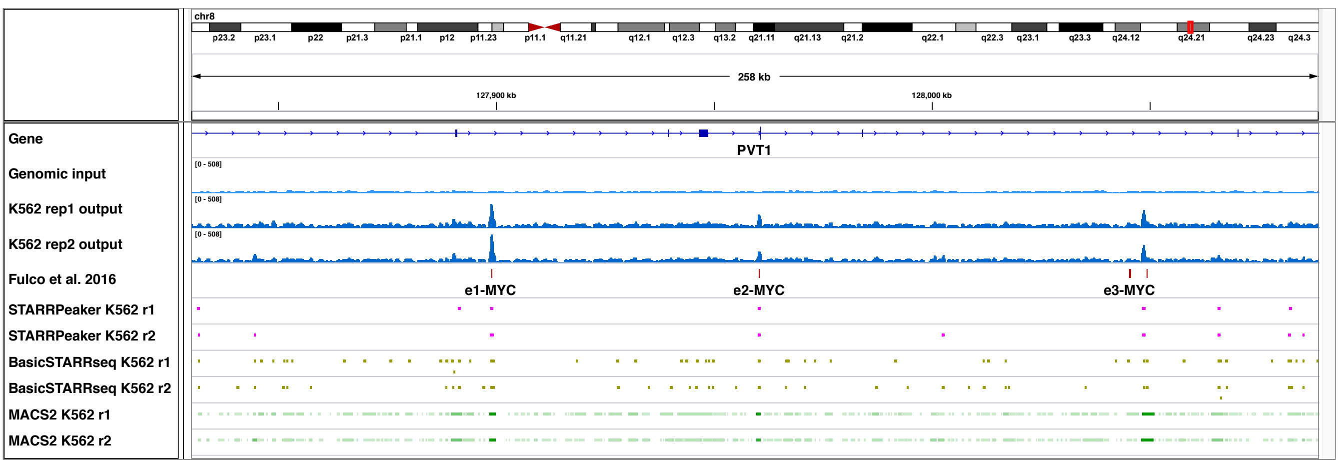

C MYC locus chr8:129550000-129720000

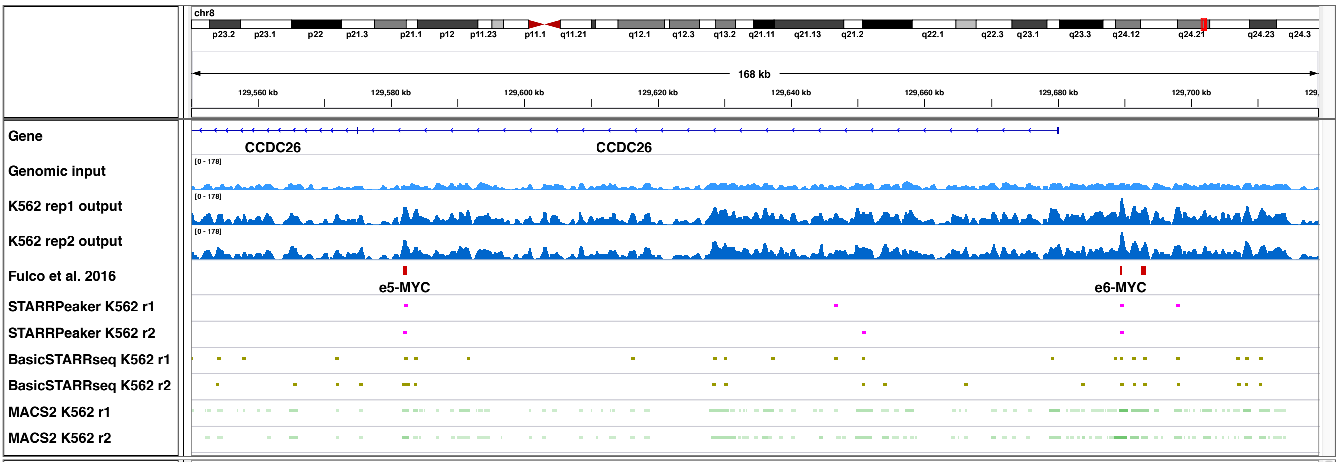

bioRxiv preprint doi: https://doi.org/10.1101/694869; this version posted May 5, 2020. The copyright holder for this preprint (which was not certified by peer review) is the author/funder, who has granted bioRxiv a license to display the preprint in perpetuity. It is made available under aCC-BY-NC-ND 4.0 International license.

Supplementary Figure 9

A

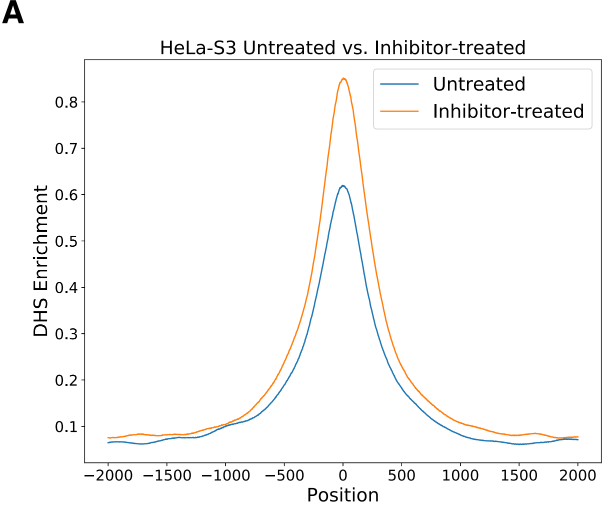

B

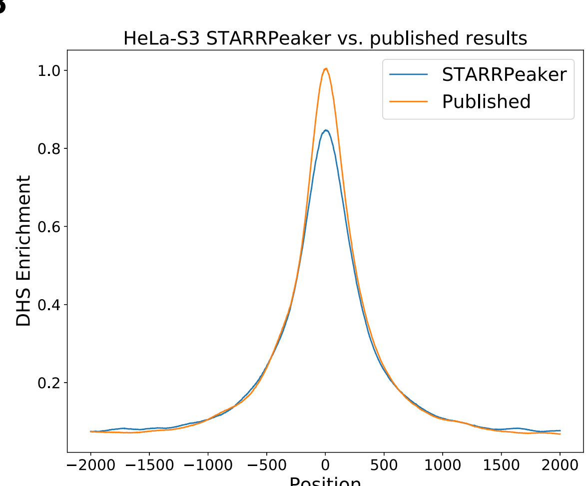

bioRxiv preprint doi: https://doi.org/10.1101/694869; this version posted May 5, 2020. The copyright holder for this preprint (which was not certified by peer review) is the author/funder, who has granted bioRxiv a license to display the preprint in perpetuity. It is made available under aCC-BY-NC-ND 4.0 International license.

Supplementary Figure 10